

# Exploring Transfer Learning in Medical Image Segmentation using Vision-Language Models

Kanchan Poudel\* Manish Dhakal\* Prasiddha Bhandari\* Rabin Adhikari\*  
Safal Thapaliya\* Bishesh Khanal

NepAI Applied Mathematics and Informatics Institute for research (NAAMII)  
{kanchan.poudel,manish.dhakal,prasiddha.bhandari,rabin.adhikari,  
safal.thapaliya,bishesh.khanal}@naamii.org.np

## Abstract

Medical Image Segmentation is crucial in various clinical applications within the medical domain. While state-of-the-art segmentation models have proven effective, integrating textual guidance to enhance visual features for this task remains an area with limited progress. Existing segmentation models that utilize textual guidance are primarily trained on open-domain images, raising concerns about their direct applicability in the medical domain without manual intervention or fine-tuning.

To address these challenges, we propose using multimodal vision-language models for capturing semantic information from image descriptions and images, enabling the segmentation of diverse medical images. This study comprehensively evaluates existing vision language models across multiple datasets to assess their transferability from the open domain to the medical field. Furthermore, we introduce variations of image descriptions for previously unseen images in the dataset, revealing notable variations in model performance based on the generated prompts.

Our findings highlight the distribution shift between the open-domain images and the medical domain and show that the segmentation models trained on open-domain images are not directly transferrable to the medical field. But their performance can be increased by finetuning them in the medical datasets. We report the zero-shot and finetuned segmentation performance of 4 Vision Language Models (VLMs) on 11 medical datasets using 9 types of prompts derived from 14 attributes.

## 1 Introduction

Medical image segmentation is essential in clinical workflow for diverse applications such as computer-aided diagnosis, prognosis, surgery planning, or population-based studies. Supervised deep learning based on Convolutional Neural Networks (CNNs) and Vision Transformers (ViTs) [8] have shown promising results in well-curated datasets across almost all imaging modalities, anatomies, and diseases [4, 11, 12, 15, 28, 30, 35, 48, 55]. However, deep learning models still face difficulties in clinical settings as they are not robust against domain shifts and are difficult to adapt when new classes are introduced. In applications except for extensive population-based studies, clinicians mostly resort to manual or semi-automated interactive segmentation approaches. Thus, improving the speed and quality of the interactive segmentation can substantially impact the clinical workflow and healthcare service delivery. Recently, the introduction of vision-language models (VLMs) [9, 17, 25, 33, 41, 52] has opened up an opportunity to use language prompts for image segmentation [13, 27, 34, 46]. Using language prompts is attractive in clinical settings because radiologists could segment complex shapes by providing only a few words in seconds; compared to visual prompts such as points or boxes,

---

\*Equal Contribution

language prompts from experts are, by design, more interpretable or explainable and can capture complex information regarding texture, shape, and spatial relationships of normal and abnormal structures; and quickly adapt to new classes.

VLMs consist of a text encoder and an image encoder with a coupling mechanism to integrate the information from both encoders. The encoders are trained to learn the image and text features jointly or separately, referred to as Vision-Language pretraining. Vision-Language pretraining has primarily been done with natural images due to the availability of many paired text and images [26, 31, 37, 39, 41]. For segmentation tasks, Vision Language Segmentation Models (VLSMs) build upon the VLMs, usually by training a decoder network to produce a segmentation mask from the embeddings learned by VLM encoders.

While there have been attempts to train VLMs from scratch using only medical images [54], most methods currently use transfer learning approaches for medical images by leveraging the VLMs trained on natural images [6, 38, 47, 50, 53]. Generating numerous manual language prompts and the corresponding medical image segmentation is impractical. Thus, Visual Question Answering (VQA) models have been explored to generate language prompts for medical images by either adapting VQA models of natural languages or training radiology VQA models from existing descriptions such as radiology reports or medical images with captions from the Internet [7, 45]. Yuksekogonul et al. [51] show that the VLMs may not have learned the intended complex relationship between the language prompt and images. Such studies are valuable to understand the limitations of current approaches in using VLMs and VQAs, and to help build better models. Qin et al. [32] evaluate how well VLMs trained in natural images adapt to object detection in medical images and show exciting results in zero-shot settings and with finetuning. However, it is unclear how well VLMs can be adapted to segmentation tasks in medical imaging; to our knowledge, no work has evaluated or proposed medical VLSMs built on natural image-trained VLMs or VLSMs.

The performance of VLSMs depends on the different types of language prompts used, target foreground masks, and datasets. We evaluate 9 types of prompts using 14 attributes, 1 VQA model, and 4 VLMs on 11 datasets in zero-shot and fine-tuning settings.

## 2 Vision Language Models (VLMs) for Medical Image Segmentation

### 2.1 Vision Language Pretraining and Foundation Models

Recently proposed foundation VLMs have a transformer-based text encoder and an image encoder, jointly trained using many online images and text pairs. A popular VLM, CLIP [33] uses contrastive language-image pretraining to jointly learn the language and the image embeddings such that they maximize predicting correct language-image pairs with 400M data pairs. Instead of contrastive learning, FLAVA [41] adds another multimodal encoder that inputs the embeddings from individual encoders and trains the model using different loss functions corresponding to vision, language, and multimodal tasks. Other VLMs such as BLIP [23], ALIGN [17], DeCLIP [25], and Locked-image Tuning (LiT) [52] are similar to CLIP, but attempt to address some of the issues such as the requirement of a large number of image-language pairs, noisy image-text pairs, and high computational complexity.

Foundation VLMs for medical imaging applications in the literature primarily build upon the VLMs pretrained on natural images using one of two approaches: (1) fine-tune a pre-trained VLM with medical image-text pairs or (2) pre-train the VLM of the same architecture from scratch with image-text pairs. BiomedCLIP [53] is a VLM obtained from contrastive pretraining from scratch on 15 million text-image pairs extracted from medical articles and journals. Seibold et al. [38] and Wu et al. [50] propose pretraining with chest radiology image-report pairs to represent the images and report entities in the same feature space. Similarly, MedCLIP [47] decoupled the two encoders of CLIP and trained them on unpaired images and texts.

Although these foundation models are intended to be helpful for a wide range of downstream tasks, their general approach to learning an embedding that aligns the whole image to the entire input text with global embedding is sub-optimal for dense prediction tasks like segmentation.

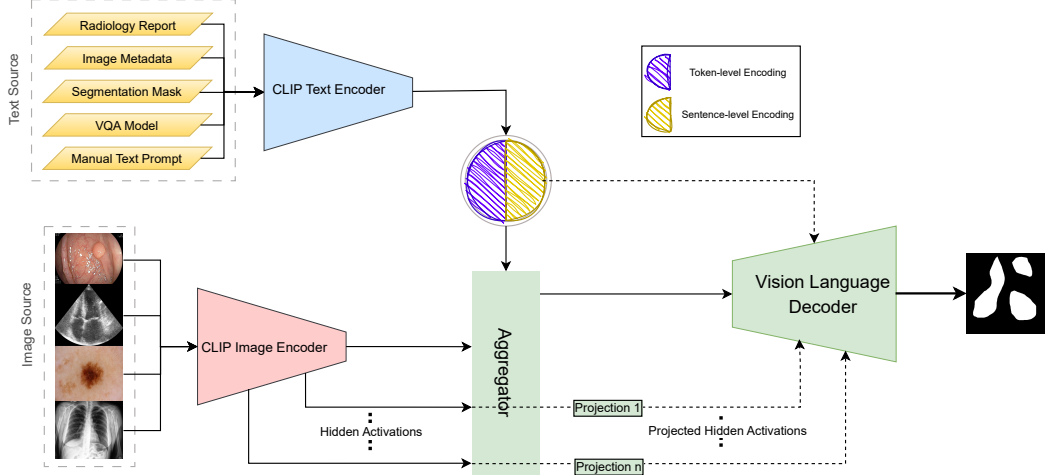


Figure 1: **The basic architecture of CRIS and CLIPSeg/BiomedCLIPSeg\* VLSMs.** The key components in the architecture are a Text Encoder, an Image Encoder, a Vision-Language Decoder (VLD), and an Aggregator. The image is fed from one of the sources to the CLIP image encoder, along with the corresponding prompt extracted from various sources. The Aggregator generates intermediate representations utilizing image-level, sentence-level, or word-level representations to feed to the Vision-Language Decoder. The dotted lines in the above figures show the optional paths specific to architecture, and the green color signifies the blocks updated during finetuning.

## 2.2 Vision Language Segmentation Models (VLSMs) with Pixel-Token alignment

Segmentation tasks may benefit more from explicitly aligning. Recent state-of-the-art VLSMs extend CLIP to segmentation tasks by adding a decoder trained to produce a segmentation map from CLIP’s vision and language embeddings. DenseCLIP [34] has proposed vision language decoders on top of the CLIP encoders that use the pixel-text score maps of the limited class prompts. In contrast to DenseCLIP, CLIPSeg [27] and CRIS [46] enforce zero-shot segmentations by giving the output as pixel-level activations for the given text or image prompt. ZegCLIP [56] has introduced tune prompts and associated the image information to the text encodings before patch-text contrasting to reduce the seen classes’ overfit.

Although there are some specific architectures to learn joint embeddings from image and text prompts for particular datasets, such as TGANet [43] for polyps, there is little work on VLSM-based medical image segmentation. Similar to Qin et al. [32], which fine-tuned GLIP [24] to ground the auto-generated medical prompts with images for object detection, a decoder can be added to BioMedCLIP [53] and fine-tune it for medical images, or VLSMs like CLIPSeg [27] and CRIS [46] can be fine-tuned to medical images.

## 3 Method

### 3.1 Contrastive Language-Image Pretraining (CLIP) models for Medical Image Segmentation

As shown in Figure 1, we have used the contrastive features representations obtained from the text and the image encoder of CLIP [33] and BiomedCLIP [53]; we projected them onto the vision language decoder to generate the binary segmentation mask. Since CLIPSeg [27], CRIS [46], and BiomedCLIP give state-of-the-art results in different vision-language tasks of natural and medical images; we have investigated the various combinations of them for implementing the VLSMs. We have defined two variants of *BiomedCLIPSeg* which have been formed by combining the pre-trained encoders of BiomedCLIP and the decoder of CLIPSeg: (1) BiomedCLIPSeg-D having the pretrained decoder of the CLIPSeg, (2) BiomedCLIPSeg having the randomly initialized decoder. CLIPSeg and CRIS models have been used for the zero-shot segmentation and fine-tuning approach. In contrast, additional BiomedCLIPSeg and BiomedCLIPSeg-D have been used only for the latter approach because they lack a pretrained vision-language decoder.

### 3.2 Datasets

We evaluate the CLIP-based models mentioned above using various 2D imaging modalities, pathologies, and organs grouped into two categories. (1) Non-radiology images comprising colon endoscopy and skin images and (2) Radiological images containing ultrasound and X-ray images (Table 1). These datasets together cover both binary and multi-class segmentation tasks.

Table 1: An overview of our datasets compared across the dimensions of category, modality, organ, foreground classes, and their splits. The datasets with multiple foreground classes signify the multi-class segmentation tasks.

Category	Modality	Organ	Name	Foreground Classes	# train/val/test
Non-Radiology	Endoscopy	Colon	Kvasir-SEG [16] ClinicDB [3] BKAI [2, 29] ETIS [40] ColonDB [42] CVC300 [44]	Polyp	800/100/100 490/61/61 800/100/100 0/0/196 0/0/380 0/0/60
	Photography	Skin Foot	ISIC [10] DFU [20]	Skin Lesion Ulcer	810/90/379 1600/200/200
Radiology	Ultrasound	Heart Breast	CAMUS [22] BUSI [1]	Myocardium, Left ventricular, and Left atrium cavity Benign and Malignant Tumors	4320/540/540 624/78/78
	X-Ray	Chest	CheXlocalize [36]	Atelectasis, Cardiomegaly, Consolidation, Edema, Enlarged Cardiomediastinum, Lung Lesion, Lung Opacity, Pleural Effusion, Pneumothorax, and Support Devices	1330/420/427

### 3.3 Prompting Engineering

Table 2: Different prompts are formed for each dataset using combinations of 14 potential attributes. Some attributes, like Pathology, are specific to some particular datasets, while others, like Class Keywords, are common to all the datasets.

Attributes → **a1**: Class Keyword, **a2**: Shape, **a3**: Color, **a4**: Size, **a5**: Number, **a6**: Location, **a7**: General Class Info, **a8**: View, **a9**: Pathology, **a10**: Cardiac Cycle, **a11**: Gender, **a12**: Age, **a13**: Image Quality, **a14**: Tumor Type

Prompt → Dataset ↓	P1	P2	P3	P4	P5	P6	P7	P8	P9
<b>Non-Radiology</b>	a1	a1a2	a1a2a3	a1a2a3a4	a1a2a3a4a5	a1a2a3a4a6	a1a7	a1a2a3a4a5a7	a1a2a3a4a5a6a7
Example Prompt	<b>P9</b> → one small pink round polyp which is often a bumpy flesh in rectum located in center of the image								
<b>CheXlocalize</b>	a1	a1a8	a1a2a8	a1a2a6a8	a1a2a6a8a9	a1a9	N/A	N/A	N/A
Example Prompt	<b>P5</b> → Airspace Opacity of shape rectangle, and located in right of the frontal view of a Chest Xray. Enlarged Cardiomediastinum, Cardiomegaly, Lung Opacity, Consolidation, Atelectasis, Pleural Effusion are present.								
<b>CAMUS</b>	a1	a1a8	a1a8a10	a1a8a10a11	a1a8a10a11a12	a1a8a10a11a12a13	a1a8a10a11a12a13a2	N/A	N/A
Example Prompt	<b>P7</b> → Left ventricular cavity of triangular shape in two-chamber view in the cardiac ultrasound at the end of the diastole cycle of a 40-year-old female with poor image quality.								
<b>BUSI</b>	a1	a1a14	a1a14a5	a1a14a5a4	a1a14a5a4a6	a1a14a5a4a6a2	N/A	N/A	N/A
Example Prompt	<b>P6</b> → Two medium square-shaped benign tumors at the center, left in the breast ultrasound image.								

Language prompt provides powerful flexibility to describe images and provide context, potentially creating a more robust and rich interactive segmentation. Better design of prompts has shown improved object detection in medical images using transfer learning of natural image VLMs [32]. As seen in Table 2, we define 14 different attributes that are relevant to various datasets (**a1-a14**) and nine combinations of the attributes which are provided as language prompts (**P1-P9**). To evaluate if the prompts boost the performance, we introduced **P0**, which refers to no language prompt (an empty prompt). The actual values of the attributes to generate input image-specific language prompts are automatically generated using different sources of information as follows.

1. **Radiology report**: It is used for the CheXlocalize dataset to get pathologies (**a9**)<sup>2</sup>.
2. **Image Metadata**: It is used for the radiology images to get **a8** (view), **a10** (cardiac cycle), **a11** (gender), **a12** (age), **a13** (image quality), and **a14** (tumor type)
3. **Segmentation mask**: It is used to get **a4** (size), **a5** (number), and **a6** (location).
4. **VQA Model**: We used OFA VQA [45] to get **a2** (shape) and **a3** (size).

<sup>2</sup>We used the pathologies given in the CheXpert dataset [14], which uses free text radiology reports for automated pathology extraction.

## 4 Experiments and Results

### 4.1 Implementation Details

Unless specified, we used the default set of parameters mentioned in the original implementation by respective authors for all the experiments. The models were fine-tuned and inferred in NVIDIA GeForce RTX 3090 and Titan Xp GPUs. We use the 16-bit mixed-precision training for the models with a batch size of 16, whenever possible, to train faster and use less memory.

CRIS’s checkpoints were finetuned using Adam [21] optimizer with the learning rate of  $10^{-5}$  and  $10^{-6}$  for the decoder and two encoders (text and vision), respectively.

The models CLIPSeg, BiomedCLIPSeg, and BiomedCLIPSeg-D have been trained by keeping the image encoder and text encoder frozen, and only the vision-language decoder was finetuned. We initially employed the same optimizer as above with a learning rate of  $10^{-3}$  and reduced it to  $10^{-4}$  if overshooting occurred.

### 4.2 Zero-shot and finetuning on Radiology Images

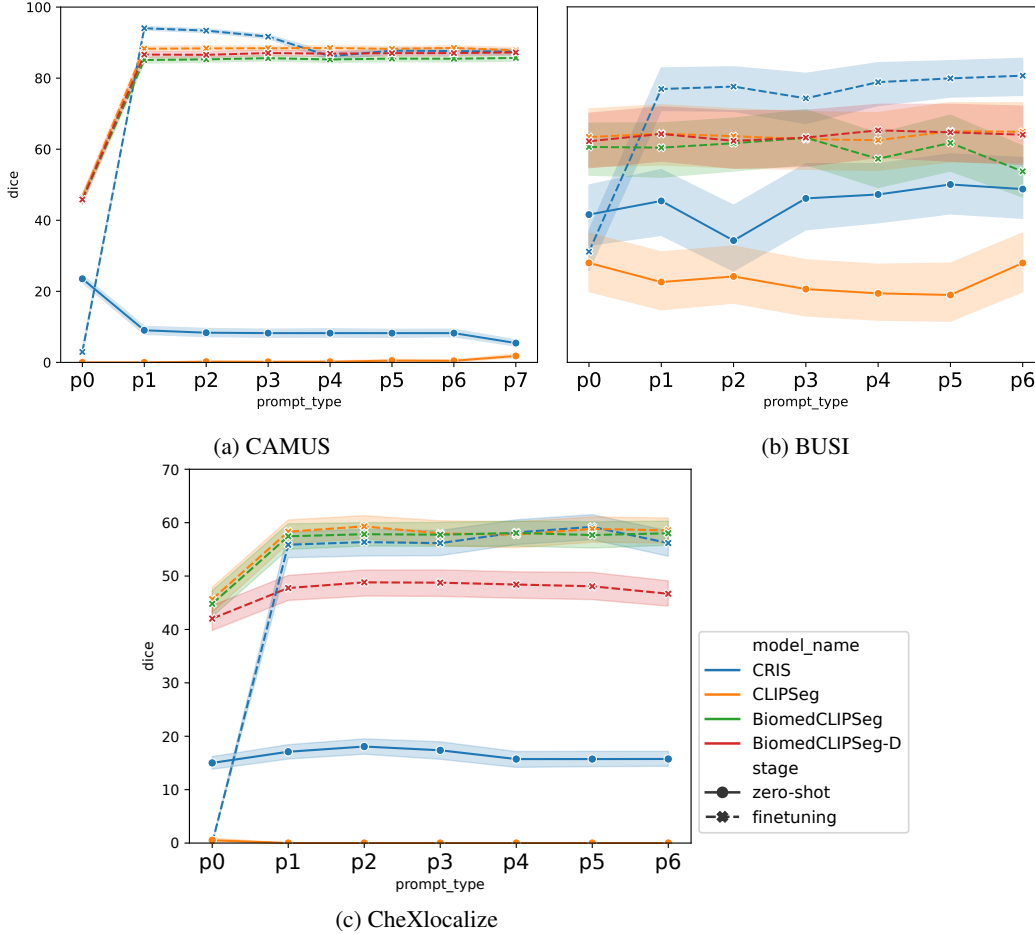


Figure 2: Zero-shot and finetuning performance of CRIS, CLIPSeg, BiomedCLIPSeg, and BiomedCLIPSeg-D model on radiology datasets. Finetuning using the prompts shows performance improvement compared to the empty prompt, which is more prominent in multiclass settings. However, using the label name and adding additional prompts does not significantly affect the model performance.

Figure 2 shows the dice scores of CRIS, CLIPSeg, BiomedCLIPSeg, and BiomedCLIPSeg-D on three radiology datasets: CAMUS, BUSI, and CheXlocalize.

We can see that CRIS outperforms CLIPSeg for radiology datasets during zero-shot. Although both the models are trained on open-domain datasets (CLIPSeg on Phrasecut [49] and CRIS on COCO [26]), the superiority of CRIS on the radiology dataset may be because textual information is more valuable in radiology to segment the images than in other domains. CRIS’ architecture focuses on preserving textual intervention at refined and granular levels.

During fine-tuning, the zero-prompted CRIS model has a lower dice score than CLIPSeg-based models. When only the class keyword is provided, the CRIS model outperforms the CLIPSeg-based models. Also, providing extra information than the class keyword doesn’t seem to have improved the performance during finetuning. Maybe this indicates that the models weren’t pretrained to capture that fine-grained medical information, or we need to fine-tune on datasets with large samples.

For the multi-class datasets, i.e., CAMUS and CheXlocalize, we changed the mask containing multiple classes to multiple binary masks for the current setting. For those datasets, the difference between the prompts **P0** and **P1** seems more prominent. This leads to a hypothesis that making the model predict different masks without providing the class information has made the model more uncertain.

### 4.3 Zero-shot and fine-tuning on Photography Images

As expected, prompting seems to have improved segmentation in photographic images compared to radiology images because the models were trained on natural images. Figure 3 shows that adding attributes in prompts significantly affects performance during zero-shot settings more than fine-tuning. Addition of information about numbers and location (**P5** and **P6**) seems to have been the most useful to CRIS, whereas the addition of general descriptions (**P7**) about the class has degraded chiefly the performance. Conversely, the attributes’ effect has not been consistent across models for different datasets for CLIPSeg. But, a more detailed analysis of zero-shot results shows prompting might not have always been helpful in CRIS. In some datasets, prompting indeed has made segmentation better. But over-segmenting imprecisely in datasets with large masks has also led to seemingly better performance (More details in supplementary section). Figure 4 demonstrates that the average gain of dice by models in the datasets can be minimal compared to the dies of a trivial classifier that segments the entire image as a target.

We also evaluated whether prompting makes it easier for the models to generalize across datasets from unseen distributions. Figure 5 shows that for CRIS, the addition of attributes to prompt, except the general description of the class, helps to improve the model’s performance in cross-dataset tests whereas, for CLIPSeg, the addition of prompts does not seem to add much value.

### 4.4 Fine tuning on a single pool of all photographic images

Table 3 shows the results for finetuning a model by combining three datasets to obtain a single training pooled dataset (Kvasir-SEG, ClinincDB, and BKAI polyp). Prompts **P0**, **P6**, and **P9** were used to capture extreme as well as average cases of prompting. But we did not find a significant gain in performance in using pooled datasets compared to the individual datasets.

Table 3: Dice score on different test splits of endoscopy datasets for CRIS model finetuned on the mixed datasets of Kvasir-SEG, ClinincDB, and BKAI.

<b>Prompt →</b> <b>Dataset ↓</b>	<b>P0</b>	<b>P6</b>	<b>P9</b>
<b>Kvasir-SEG</b>	14.61 $\pm$ 19.43	<b>89.41</b> $\pm$ 14.14	88.95 $\pm$ 14.91
<b>Clinicdb</b>	18.43 $\pm$ 23.27	<b>85.99</b> $\pm$ 19.51	83.19 $\pm$ 24.16
<b>BKAI</b>	13.67 $\pm$ 20.25	<b>85.29</b> $\pm$ 21.83	83.07 $\pm$ 25.21
<b>CVC300</b>	11.27 $\pm$ 19.73	85.39 $\pm$ 19.26	<b>86.03</b> $\pm$ 16.95
<b>ColonDB</b>	6.81 $\pm$ 15.05	73.6 $\pm$ 30.55	<b>74.23</b> $\pm$ 29.98
<b>ETIS</b>	3.67 $\pm$ 11.61	<b>71.73</b> $\pm$ 30.8	67.71 $\pm$ 32.84

By observing the results from Tables 3 and 4, we can see there is no significant difference between the presence and absence of the prompts for the in-distribution datasets. But, it also shows some improvement for the out-of-distribution datasets. It shows that we can leverage the prompting

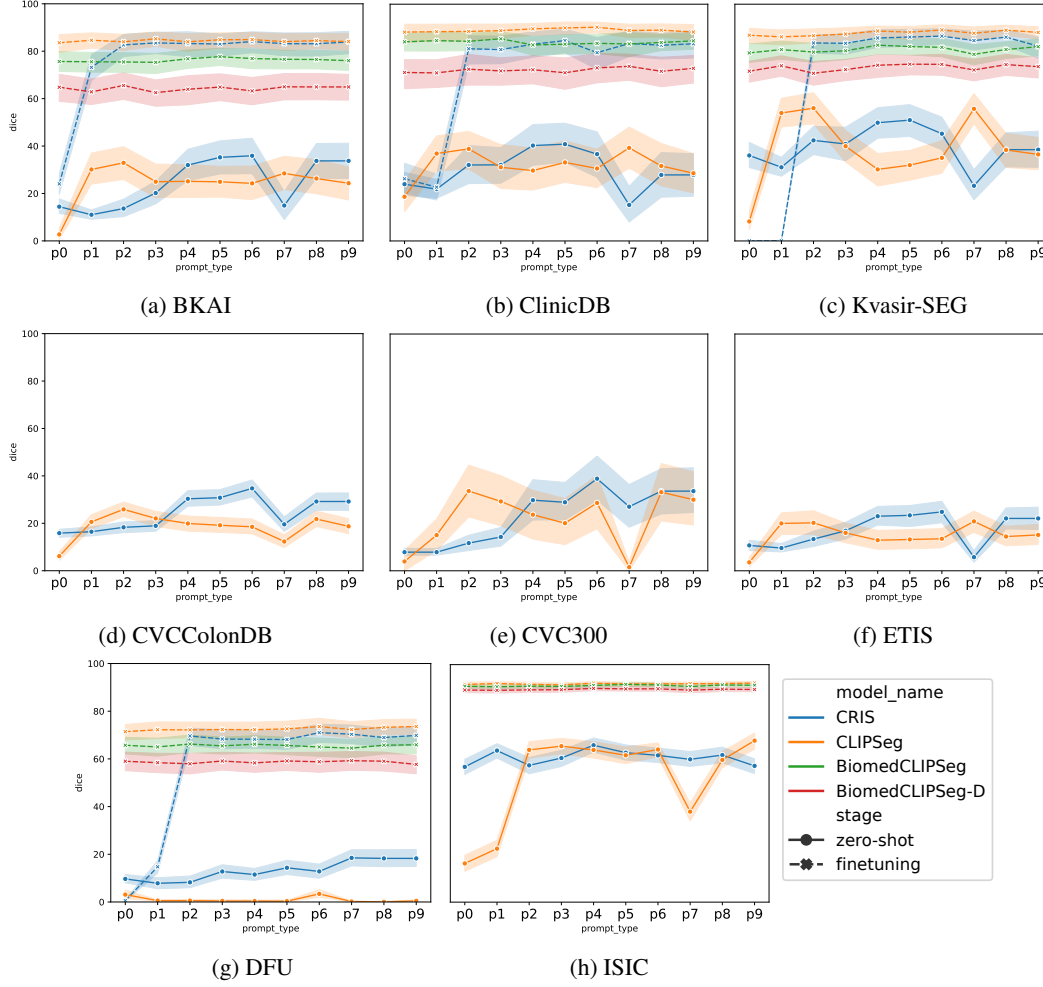


Figure 3: Dice scores of CRIS, CLIPSeg, BiomedCLIPSeg, and BiomedCLIPSeg-D on three photography datasets: Kvasir-SEG, ClinicDB, BKA I Polyp, CVC300, CVCColonDB, ETIS-Larib, DFU, and ISIC

Table 4: Dice score on different test splits of endoscopy datasets for CLIPSeg model fine-tuned on the mixed datasets of Kvasir-SEG, ClinicDB, and BKA I.

Prompt → Dataset ↓	P0	P6	P9
<b>Kvasir-SEG</b>	87.11 $\pm$ 16.51	<b>89.01</b> $\pm$ 13.69	88.54 $\pm$ 14.62
<b>Clinicdb</b>	<b>90.76</b> $\pm$ 7.77	90.23 $\pm$ 8.83	89.93 $\pm$ 11.69
<b>BKA I</b>	<b>86.43</b> $\pm$ 13.79	84.78 $\pm$ 17.5	85.1 $\pm$ 17.3
<b>CVC300</b>	88.05 $\pm$ 12.6	<b>88.2</b> $\pm$ 14.25	88.03 $\pm$ 12.87
<b>ColonDB</b>	72.43 $\pm$ 27.85	73.1 $\pm$ 28.19	<b>74.56</b> $\pm$ 27.15
<b>ETIS</b>	66.44 $\pm$ 30.86	68.23 $\pm$ 31.29	<b>69.56</b> $\pm$ 29.95

mechanisms for adapting the segmentation tasks for the datasets with a different distribution than the training dataset.

## 5 Limitations and Future Work

While our study incorporates two Vision Language Segmentation Models (VLSMs) for medical image segmentation tasks, it is essential to acknowledge that our selection does not cover all published

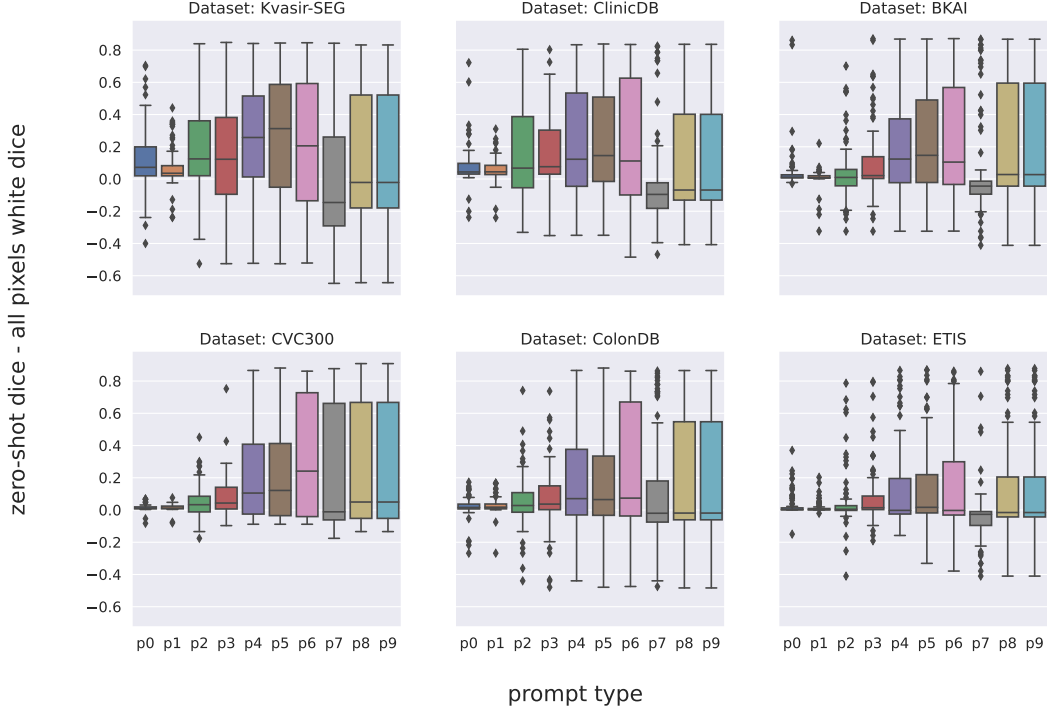


Figure 4: Difference between dice scores for zero-shot test and scores obtained by a trivial segmentation of segmenting all pixels as foreground in CRIS-trained different datasets across prompt types

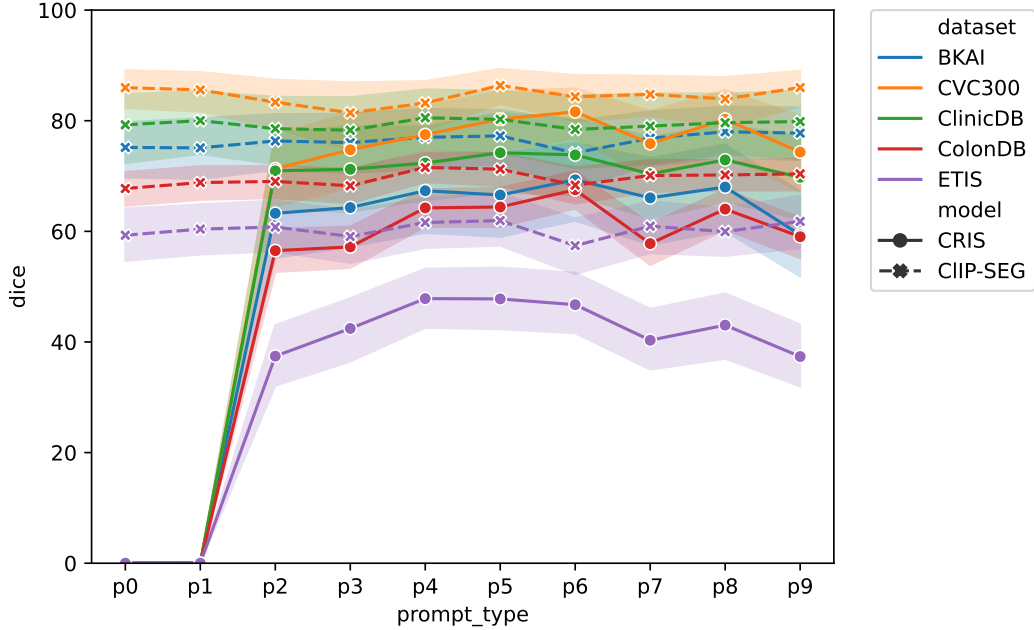


Figure 5: Performance of the model finetuned on Kvasir-SEG dataset with different prompt types on testing with other datasets.

VLSMs. Some models lacked available code [13], while discrepancies in library versions prevented the execution of others [34]. Additionally, our choice of datasets was limited to those we deemed representative of various medical modalities. Future research endeavors could explore a broader range of VLSMs and include more diverse datasets to investigate these models' performance further.



A potential limitation of our experimental setup is the reliance on prompts generated using Visual Question Answering (VQA) models. The accuracy of these prompts is contingent upon the data distribution used to train the VQA model. To improve the utility of text prompts, it would be beneficial to develop a more robust VQA model that can accurately answer open-ended questions. Additionally, manual verification of prompts by annotators could enhance their accuracy, leading to more effective VLSMs for medical images.

Considering that the datasets used in our study were limited to 2D images, it would be intriguing to explore the performance differences for 3D images, such as CT scans, when adapting VLSMs trained on 2D images. Investigating the adaptation of these models to handle 3D medical images could open up exciting avenues for future research.

## 6 Conclusion

Our research evaluated CLIPSeg [27] variants and CRIS [46] for medical image segmentation, utilizing a diverse set of medical images and prompts automatically extracted from various sources. Our findings suggest that Vision Language Models (VLMs) and prompting techniques, while successful in object detection [32], do not exhibit the same effectiveness in medical image segmentation.

We observed that VLMs trained on open-domain images could not be directly applied to the medical domain due to the significant distribution shift between these domains. Notably, the models face challenges when dealing with radiology images, highlighting the difficulty posed by the domain gap. Furthermore, our results indicate that CRIS generally outperforms CLIPSeg, which may be attributed to CRIS’s emphasis on leveraging different levels of textual information.

Notably, we observed an improvement in model performance when the models were finetuned on medical images, demonstrating the learning potential of the models. However, we also observed that the performance reaches a saturation point beyond which additional information provided to the model does not significantly enhance its performance. This suggests the need for more representative samples from the medical domain in the pretraining dataset or a sufficiently large finetuning medical image dataset to increase performance further.

In conclusion, our research highlights the challenges of applying VLMs and prompting techniques to medical image segmentation, emphasizing the gap between open-domain and medical-domain images. We identify CRIS as a more promising approach and demonstrate the potential for improved performance through finetuning on medical images. Future work should focus on expanding the pretraining dataset with more representative medical samples or utilizing larger finetuning medical image datasets to enhance performance in this critical task.

## Acknowledgments and Disclosure of Funding

We thank Kathmandu University for its invaluable support in granting us access to its supercomputer infrastructure. This enabled the successful execution of the experiments crucial to this paper. We are grateful for its willingness to collaborate and commitment to advancing scientific knowledge.

## References

- [1] W. Al-Dhabyani, M. Goma, H. Khaled, and A. Fahmy. Dataset of breast ultrasound images. *Data in brief*, 28:104863, 2020.
- [2] N. S. An, P. N. Lan, D. V. Hang, D. V. Long, T. Q. Trung, N. T. Thuy, and D. V. Sang. Blazeneo: Blazing fast polyp segmentation and neoplasm detection. *IEEE Access*, 10:43669–43684, 2022.
- [3] J. Bernal, F. J. Sánchez, G. Fernández-Esparrach, D. Gil, C. Rodríguez, and F. Vilariño. Wm-dova maps for accurate polyp highlighting in colonoscopy: Validation vs. saliency maps from physicians. *Computerized medical imaging and graphics*, 43:99–111, 2015.
- [4] J. Chen, Y. Lu, Q. Yu, X. Luo, E. Adeli, Y. Wang, L. Lu, A. L. Yuille, and Y. Zhou. Transunet: Transformers make strong encoders for medical image segmentation. *arXiv preprint arXiv:2102.04306*, 2021.
- [5] L.-C. Chen, P.-C. Kuo, R. Wang, J. Gichoya, and L. A. Celi. Chest x-ray segmentation images based on mimic-cxr. 2022.

- [6] Z. Chen, S. Diao, B. Wang, G. Li, and X. Wan. Towards unifying medical vision-and-language pre-training via soft prompts. *arXiv preprint arXiv:2302.08958*, 2023.
- [7] T. Do, B. X. Nguyen, E. Tjiputra, M. Tran, Q. D. Tran, and A. Nguyen. Multiple meta-model quantifying for medical visual question answering. In *Medical Image Computing and Computer Assisted Intervention–MICCAI 2021: 24th International Conference, Strasbourg, France, September 27–October 1, 2021, Proceedings, Part V 24*, pages 64–74. Springer, 2021.
- [8] A. Dosovitskiy, L. Beyer, A. Kolesnikov, D. Weissenborn, X. Zhai, T. Unterthiner, M. Dehghani, M. Minderoeder, G. Heigold, S. Gelly, et al. An image is worth 16x16 words: Transformers for image recognition at scale. *arXiv preprint arXiv:2010.11929*, 2020.
- [9] A. Fürst, E. Rumetshofer, J. Lehner, V. T. Tran, F. Tang, H. Ramsauer, D. Kreil, M. Kopp, G. Klambauer, A. Bitto, et al. Cloob: Modern hopfield networks with infoloob outperform clip. *Advances in neural information processing systems*, 35:20450–20468, 2022.
- [10] D. Gutman, N. C. Codella, E. Celebi, B. Helba, M. Marchetti, N. Mishra, and A. Halpern. Skin lesion analysis toward melanoma detection: A challenge at the international symposium on biomedical imaging (isbi) 2016, hosted by the international skin imaging collaboration (isic). *arXiv preprint arXiv:1605.01397*, 2016.
- [11] A. Hatamizadeh, Y. Tang, V. Nath, D. Yang, A. Myronenko, B. Landman, H. R. Roth, and D. Xu. Unetr: Transformers for 3d medical image segmentation. In *Proceedings of the IEEE/CVF winter conference on applications of computer vision*, pages 574–584, 2022.
- [12] M. Havaei, A. Davy, D. Warde-Farley, A. Biard, A. Courville, Y. Bengio, C. Pal, P.-M. Jodoin, and H. Larochelle. Brain tumor segmentation with deep neural networks. *Medical image analysis*, 35:18–31, 2017.
- [13] Z. Huang, Z. Zeng, B. Liu, D. Fu, and J. Fu. Pixel-bert: Aligning image pixels with text by deep multi-modal transformers. *arXiv preprint arXiv:2004.00849*, 2020.
- [14] J. Irvin, P. Rajpurkar, M. Ko, Y. Yu, S. Ciurea-Ilcus, C. Chute, H. Marklund, B. Haghighi, R. Ball, K. Shpanskaya, et al. Chexpert: A large chest radiograph dataset with uncertainty labels and expert comparison. In *Proceedings of the AAAI conference on artificial intelligence*, volume 33, pages 590–597, 2019.
- [15] F. Isensee, P. F. Jaeger, S. A. Kohl, J. Petersen, and K. H. Maier-Hein. nnu-net: a self-configuring method for deep learning-based biomedical image segmentation. *Nature methods*, 18(2):203–211, 2021.
- [16] D. Jha, P. H. Smedsrud, M. A. Riegler, P. Halvorsen, T. de Lange, D. Johansen, and H. D. Johansen. Kvasir-seg: A segmented polyp dataset. In *MultiMedia Modeling: 26th International Conference, MMM 2020, Daejeon, South Korea, January 5–8, 2020, Proceedings, Part II 26*, pages 451–462. Springer, 2020.
- [17] C. Jia, Y. Yang, Y. Xia, Y.-T. Chen, Z. Parekh, H. Pham, Q. Le, Y.-H. Sung, Z. Li, and T. Duerig. Scaling up visual and vision-language representation learning with noisy text supervision. In *International Conference on Machine Learning*, pages 4904–4916. PMLR, 2021.
- [18] A. E. Johnson, T. J. Pollard, S. J. Berkowitz, N. R. Greenbaum, M. P. Lungren, C.-y. Deng, R. G. Mark, and S. Horng. MIMIC-CXR, a de-identified publicly available database of chest radiographs with free-text reports. *Scientific data*, 6(1):317, 2019.
- [19] A. E. Johnson, T. J. Pollard, N. R. Greenbaum, M. P. Lungren, C.-y. Deng, Y. Peng, Z. Lu, R. G. Mark, S. J. Berkowitz, and S. Horng. MIMIC-CXR-JPG, a large publicly available database of labeled chest radiographs. *arXiv preprint arXiv:1901.07042*, 2019.
- [20] C. Kendrick, B. Cassidy, J. M. Pappachan, C. O’Shea, C. J. Fernandez, E. Chacko, K. Jacob, N. D. Reeves, and M. H. Yap. Translating clinical delineation of diabetic foot ulcers into machine interpretable segmentation. *arXiv preprint arXiv:2204.11618*, 2022.
- [21] D. P. Kingma and J. Ba. Adam: A method for stochastic optimization, 2017.
- [22] S. Leclerc, E. Smistad, J. Pedrosa, A. Østvik, F. Cervenansky, F. Espinosa, T. Espeland, E. A. R. Berg, P.-M. Jodoin, T. Grenier, et al. Deep learning for segmentation using an open large-scale dataset in 2d echocardiography. *IEEE transactions on medical imaging*, 38(9):2198–2210, 2019.
- [23] J. Li, D. Li, C. Xiong, and S. Hoi. Blip: Bootstrapping language-image pre-training for unified vision-language understanding and generation. In *International Conference on Machine Learning*, pages 12888–12900. PMLR, 2022.

- [24] L. H. Li, P. Zhang, H. Zhang, J. Yang, C. Li, Y. Zhong, L. Wang, L. Yuan, L. Zhang, J.-N. Hwang, et al. Grounded language-image pre-training. In *Proceedings of the IEEE/CVF Conference on Computer Vision and Pattern Recognition*, pages 10965–10975, 2022.
- [25] Y. Li, F. Liang, L. Zhao, Y. Cui, W. Ouyang, J. Shao, F. Yu, and J. Yan. Supervision exists everywhere: A data efficient contrastive language-image pre-training paradigm. *arXiv preprint arXiv:2110.05208*, 2021.
- [26] T.-Y. Lin, M. Maire, S. Belongie, J. Hays, P. Perona, D. Ramanan, P. Dollár, and C. L. Zitnick. Microsoft coco: Common objects in context. In *Computer Vision—ECCV 2014: 13th European Conference, Zurich, Switzerland, September 6–12, 2014, Proceedings, Part V 13*, pages 740–755. Springer, 2014.
- [27] T. Lüddecke and A. Ecker. Image segmentation using text and image prompts. In *Proceedings of the IEEE/CVF Conference on Computer Vision and Pattern Recognition*, pages 7086–7096, 2022.
- [28] F. Milletari, N. Navab, and S.-A. Ahmadi. V-net: Fully convolutional neural networks for volumetric medical image segmentation. In *2016 fourth international conference on 3D vision (3DV)*, pages 565–571. Ieee, 2016.
- [29] P. Ngoc Lan, N. S. An, D. V. Hang, D. V. Long, T. Q. Trung, N. T. Thuy, and D. V. Sang. Neounet: Towards accurate colon polyp segmentation and neoplasm detection. In *Advances in Visual Computing: 16th International Symposium, ISVC 2021, Virtual Event, October 4–6, 2021, Proceedings, Part II*, pages 15–28. Springer, 2021.
- [30] O. Oktay, J. Schlemper, L. L. Folgoc, M. Lee, M. Heinrich, K. Misawa, K. Mori, S. McDonagh, N. Y. Hammerla, B. Kainz, et al. Attention u-net: Learning where to look for the pancreas. *arXiv preprint arXiv:1804.03999*, 2018.
- [31] B. A. Plummer, L. Wang, C. M. Cervantes, J. C. Caicedo, J. Hockenmaier, and S. Lazebnik. Flickr30k entities: Collecting region-to-phrase correspondences for richer image-to-sentence models. In *Proceedings of the IEEE international conference on computer vision*, pages 2641–2649, 2015.
- [32] Z. Qin, H. Yi, Q. Lao, and K. Li. Medical image understanding with pretrained vision language models: A comprehensive study. *arXiv preprint arXiv:2209.15517*, 2022.
- [33] A. Radford, J. W. Kim, C. Hallacy, A. Ramesh, G. Goh, S. Agarwal, G. Sastry, A. Askell, P. Mishkin, J. Clark, et al. Learning transferable visual models from natural language supervision. In *International conference on machine learning*, pages 8748–8763. PMLR, 2021.
- [34] Y. Rao, W. Zhao, G. Chen, Y. Tang, Z. Zhu, G. Huang, J. Zhou, and J. Lu. Denseclip: Language-guided dense prediction with context-aware prompting. In *Proceedings of the IEEE/CVF Conference on Computer Vision and Pattern Recognition*, pages 18082–18091, 2022.
- [35] O. Ronneberger, P. Fischer, and T. Brox. U-net: Convolutional networks for biomedical image segmentation. In *Medical Image Computing and Computer-Assisted Intervention—MICCAI 2015: 18th International Conference, Munich, Germany, October 5–9, 2015, Proceedings, Part III 18*, pages 234–241. Springer, 2015.
- [36] A. Saporta, X. Gui, A. Agrawal, A. Pareek, S. Q. Truong, C. D. Nguyen, V.-D. Ngo, J. Seekins, F. G. Blankenberg, A. Y. Ng, et al. Benchmarking saliency methods for chest x-ray interpretation. *Nature Machine Intelligence*, 4(10):867–878, 2022.
- [37] C. Schuhmann, R. Beaumont, R. Vencu, C. Gordon, R. Wightman, M. Cherti, T. Coombes, A. Katta, C. Mullis, M. Wortsman, et al. Laion-5b: An open large-scale dataset for training next generation image-text models. *arXiv preprint arXiv:2210.08402*, 2022.
- [38] C. Seibold, S. Reiß, M. S. Sarfraz, R. Stiefelwagen, and J. Kleesiek. Breaking with fixed set pathology recognition through report-guided contrastive training. In *Medical Image Computing and Computer Assisted Intervention—MICCAI 2022: 25th International Conference, Singapore, September 18–22, 2022, Proceedings, Part V*, pages 690–700. Springer, 2022.
- [39] P. Sharma, N. Ding, S. Goodman, and R. Soricut. Conceptual captions: A cleaned, hypernymed, image alt-text dataset for automatic image captioning. In *Proceedings of the 56th Annual Meeting of the Association for Computational Linguistics (Volume 1: Long Papers)*, pages 2556–2565, 2018.
- [40] J. Silva, A. Histace, O. Romain, X. Dray, and B. Granado. Toward embedded detection of polyps in wce images for early diagnosis of colorectal cancer. *International journal of computer assisted radiology and surgery*, 9:283–293, 2014.

- [41] A. Singh, R. Hu, V. Goswami, G. Couairon, W. Galuba, M. Rohrbach, and D. Kiela. Flava: A foundational language and vision alignment model. In *Proceedings of the IEEE/CVF Conference on Computer Vision and Pattern Recognition*, pages 15638–15650, 2022.
- [42] N. Tajbakhsh, S. R. Gurudu, and J. Liang. Automated polyp detection in colonoscopy videos using shape and context information. *IEEE transactions on medical imaging*, 35(2):630–644, 2015.
- [43] N. K. Tomar, D. Jha, U. Bagci, and S. Ali. Tganet: text-guided attention for improved polyp segmentation. In *Medical Image Computing and Computer Assisted Intervention–MICCAI 2022: 25th International Conference, Singapore, September 18–22, 2022, Proceedings, Part III*, pages 151–160. Springer, 2022.
- [44] D. Vázquez, J. Bernal, F. J. Sánchez, G. Fernández-Esparrach, A. M. López, A. Romero, M. Drozdal, and A. Courville. A benchmark for endoluminal scene segmentation of colonoscopy images. *Journal of healthcare engineering*, 2017, 2017.
- [45] P. Wang, A. Yang, R. Men, J. Lin, S. Bai, Z. Li, J. Ma, C. Zhou, J. Zhou, and H. Yang. Ofa: Unifying architectures, tasks, and modalities through a simple sequence-to-sequence learning framework. In *International Conference on Machine Learning*, pages 23318–23340. PMLR, 2022.
- [46] Z. Wang, Y. Lu, Q. Li, X. Tao, Y. Guo, M. Gong, and T. Liu. Cris: Clip-driven referring image segmentation. In *Proceedings of the IEEE/CVF conference on computer vision and pattern recognition*, pages 11686–11695, 2022.
- [47] Z. Wang, Z. Wu, D. Agarwal, and J. Sun. Medclip: Contrastive learning from unpaired medical images and text. *arXiv preprint arXiv:2210.10163*, 2022.
- [48] S. Wazir and M. M. Fraz. Histoseg: Quick attention with multi-loss function for multi-structure segmentation in digital histology images. In *2022 12th International Conference on Pattern Recognition Systems (ICPRS)*, pages 1–7. IEEE, 2022.
- [49] C. Wu, Z. Lin, S. Cohen, T. Bui, and S. Maji. Phrasecut: Language-based image segmentation in the wild. In *Proceedings of the IEEE/CVF Conference on Computer Vision and Pattern Recognition*, pages 10216–10225, 2020.
- [50] C. Wu, X. Zhang, Y. Zhang, Y. Wang, and W. Xie. Medkclip: Medical knowledge enhanced language-image pre-training. *medRxiv*, pages 2023–01, 2023.
- [51] M. Yuksekgonul, F. Bianchi, P. Kalluri, D. Jurafsky, and J. Zou. When and why vision-language models behave like bag-of-words models, and what to do about it? *arXiv preprint arXiv:2210.01936*, 2022.
- [52] X. Zhai, X. Wang, B. Mustafa, A. Steiner, D. Keysers, A. Kolesnikov, and L. Beyer. Lit: Zero-shot transfer with locked-image text tuning. In *Proceedings of the IEEE/CVF Conference on Computer Vision and Pattern Recognition*, pages 18123–18133, 2022.
- [53] S. Zhang, Y. Xu, N. Usuyama, J. Bagga, R. Tinn, S. Preston, R. Rao, M. Wei, N. Valluri, C. Wong, et al. Large-scale domain-specific pretraining for biomedical vision-language processing. *arXiv preprint arXiv:2303.00915*, 2023.
- [54] Y. Zhang, H. Jiang, Y. Miura, C. D. Manning, and C. P. Langlotz. Contrastive learning of medical visual representations from paired images and text (2020). *arXiv preprint arXiv:2010.00747*, 2020.
- [55] Z. Zhou, M. M. Rahman Siddiquee, N. Tajbakhsh, and J. Liang. Unet++: A nested u-net architecture for medical image segmentation. In *Deep Learning in Medical Image Analysis and Multimodal Learning for Clinical Decision Support: 4th International Workshop, DLMIA 2018, and 8th International Workshop, ML-CDS 2018, Held in Conjunction with MICCAI 2018, Granada, Spain, September 20, 2018, Proceedings 4*, pages 3–11. Springer, 2018.
- [56] Z. Zhou, B. Zhang, Y. Lei, L. Liu, and Y. Liu. Zegclip: Towards adapting clip for zero-shot semantic segmentation. *arXiv preprint arXiv:2212.03588*, 2022.

## A Impact on Society

The incorporation of language prompts in medical image segmentation has the potential to impact society, particularly in clinical settings, significantly. By enabling radiologists to quickly and accurately segment complex shapes using just a few words, language prompts offer a more interpretable and explainable approach compared to traditional visual prompts such as points or boxes.

One significant advantage of language prompts is their ability to convey detailed information about normal and abnormal structures' texture, shape, and spatial relationships. This allows for a more comprehensive medical image understanding, facilitating more accurate segmentation results. Additionally, language prompts can be easily adapted to new classes, making them highly versatile and adaptable in various medical scenarios.

Using language prompts in medical image segmentation can improve the efficiency and effectiveness of radiologists' work, potentially leading to faster diagnoses and treatment decisions. Moreover, the interpretability of language prompts can aid in building trust and confidence among healthcare professionals and patients as the reasoning behind the segmentation process becomes more transparent.

Overall, the integration of language prompts in medical image segmentation has the potential to revolutionize clinical practices, providing radiologists with a powerful tool to enhance their segmentation capabilities and ultimately improve patient care outcomes.

We strongly encourage and invite other researchers to contribute to this field of study. This research paper has no negative impact on society or further research in medical imaging, as we have adhered to ethical considerations in medical imaging and have not expressed disapproval of any previous studies.

## B Datasets

### B.1 Dataset Access

The anonymous code for the benchmarks, along with the prompt generated, can be viewed using this link<sup>3</sup>. The images and masks used during the experiment are from publicly available images. They are not kept in the above link because they may be subject to the copyright of the respective owners.

### B.2 Prompt Composition

The prompts used during the training for various datasets are shown below. If there are multiple templates for the same prompts for a dataset, one is randomly chosen during the training to increase the regularization for the models.

#### B.2.1 Non-radiology images

**Endoscopy Datasets** A total of six endoscopy datasets (polyp segmentation image-mask pairs) have been used for fine-tuning and evaluating our proposed models: Kvasir-SEG [16], ClinicDB [3], BKAI [2, 29], CVC-300 [44], CVC-ColonDB [42], and ETIS [40]. The last three datasets have very few numbers of image-masks pairs, so they are primarily used for testing and evaluating the trained models.

1. **P0:** "" (No prompt)
2. **P1:** "*class name*"
  - *polyp*
3. **P2:** "*shape class name*"
  - *round polyp*
4. **P3:** "*color shape class name*"
  - *pink round polyp*

---

<sup>3</sup><https://anonymous.4open.science/r/VLMSEG-42E6>

5. **P4**: "size color shape class name"
  - medium pink round polyp
6. **P5**: "number size color shape class name"
  - one medium pink round polyp
7. **P6**: "number size color shape class name, located in the location of the image"
  - one medium pink round polyp, located in the top left of the image
8. **P7**: "class name, which is a general description of the class"
  - polyp, which is a small lump in the lining of colon
9. **P8**: "number size color shape class name, which is a general description of the class"
  - one medium pink round polyp, which is a small lump in the lining of colon
10. **P9**: "number size color shape class name, which is a general description of the class located in the location of the image "
  - one medium pink round polyp, which is a small lump in the lining of colon located in the top left of the image

For *General Description of the class*, prompts were built using information about the subject on the internet. Five such descriptions were designed for each dataset, and one random sample was selected each time as the *general description of the class* attribute whenever the prompts **p7**, **p8**, and **p9** were used.

**ISIC and DFU-2022** The templates of prompts for the DFU-2022 [20] and ISIC [10] datasets used were the same as the above examples for endoscopy images, with *class name* and *general description of the class* being different. We used class names **skin melanoma** and **foot ulcer** for the two datasets, respectively.

The five *General Description of the class* for each of the three types of photographic datasets used is listed in the table below.

Table 5: General Descriptions selected for each of the photographic datasets

Endoscopy Datasets	ISIC	DFU-2022
→ a projecting growth of tissue	→ a spot with dark speckles	→ a wound in foot and toes
→ often a bumpy flesh in rectum	→ a spot with irregular texture	→ a sore in foot and toes
→ a small lump in the lining of colon	→ a dark sore with irregular texture	→ a sore in skin of foot and toe
→ a tissue growth that often resemble mushroom-like stalks	→ an irregular sore with speckles	→ an abnormality in foot and toes
→ an abnormal growth of tissues projecting from a mucous membrane	→ a rough wound on skin	→ an open sore or lesion in foot and toes

## B.2.2 Radiology Images

**CheXlocalize** The prompts for the CheXlocalize [36] dataset are listed below.

1. **P0**: "" (No prompt)
2. **P1**: "labels in a chest Xray."
  - Airspace Opacity in a chest Xray.
3. **P2**: "labels in the xray\_view view of a Chest Xray."
  - Airspace Opacity in the frontal view of a Chest Xray.
4. **P3**: "labels of shape shape in the xray\_view view of a Chest Xray."
  - Airspace Opacity of shape rectangle in the frontal view of a Chest Xray.
5. **P4**: "labels of shape shape, and located in location of the xray\_view view of a Chest Xray."

- Airspace Opacity of shape rectangle, and located in *right* of the frontal view of a Chest Xray.
6. **P5:** "*labels* of shape *shape*, and located in *location* of the *xray\_view* view of a Chest Xray. *pathology* are present."
- Airspace Opacity of shape rectangle, and located in right of the frontal view of a Chest Xray. *Enlarged Cardiomeastinum, Cardiomegaly, Lung Opacity, Consolidation, Atelectasis, Pleural Effusion* are present.
7. **P6:** "*labels* in a Chest Xray. *pathology* are present."
- Airspace Opacity in a Chest Xray. *Enlarged Cardiomeastinum, Cardiomegaly, Lung Opacity, Consolidation, Atelectasis, Pleural Effusion* are present.

**CAMUS** The prompts for the CAMUS [22] dataset are listed below.

1. Class of Current Image
  - *Left ventricular cavity, Myocardium, or Left atrium cavity* of the heart
  - [*class*] in the cardiac ultrasound
2. Include the chamber information
  - Left ventricular cavity in *two-chamber view* of the heart.
  - Left ventricular cavity in *two-chamber view* in the cardiac ultrasound.
3. Include the cycle
  - Left ventricular cavity in two-chamber view of the heart at the *end of the diastole cycle*.
  - Left ventricular cavity in two-chamber view in the cardiac ultrasound at the *end of the diastole cycle*.
4. Include the gender
  - Left ventricular cavity in two-chamber view of the heart at the end of the diastole cycle of *a female*.
  - Left ventricular cavity in two-chamber view in the cardiac ultrasound at the end of the diastole cycle of *a female*.
5. Include the age
  - Left ventricular cavity in two-chamber view of the heart at the end of the diastole cycle of *a forty-six-year-old female*.
  - Left ventricular cavity in two-chamber view in the cardiac ultrasound at the end of the diastole cycle of *a forty-six-year-old female*.
6. Include the image quality
  - Left ventricular cavity in two-chamber view of the heart at the end of the diastole cycle of *a 40-year-old female with poor image quality*.
  - Left ventricular cavity in two-chamber view in the cardiac ultrasound at the end of the diastole cycle of *a 40-year-old female with poor image quality*.
7. Include the mask shape
  - Left ventricular cavity of *triangular shape* in two-chamber view of the heart at the end of the diastole cycle of *a 40-year-old female with poor image quality*.
  - Left ventricular cavity of *triangular shape* in two-chamber view in the cardiac ultrasound at the end of the diastole cycle of *a 40-year-old female with poor image quality*.

**Breast Ultrasound Images Dataset** The prompts for the Breast Ultrasound Images (BUSI) [1] dataset are listed below.

1. Presence of tumor
  - [*No*] *tumor* in the breast ultrasound image

2. Tumor Type
  - *Benign* tumor in the breast ultrasound image
  - *Regular-shaped* tumor in the breast ultrasound image
3. Tumor Number
  - *Two* benign tumors in the breast ultrasound image
  - *Two* regular-shaped tumors in the breast ultrasound image
4. Tumor Coverage
  - Two *medium* benign tumors in the breast ultrasound image
  - Two *medium* regular-shaped tumors in the breast ultrasound image
5. Tumor Location
  - Two medium benign tumors *at the center, left* in the breast ultrasound image
  - Two medium regular-shaped tumors *at the center, left* in the breast ultrasound image
6. Tumor Shape
  - Two medium *square-shaped* benign tumors at the center, left in the breast ultrasound image
  - Two medium *square-shaped* regular tumors at the center, left in the breast ultrasound image

## C Experiments

Table 6: Number of prompting mechanisms for each of the datasets that have been used in all of our experiments.

Datasets	No. of prompting mecahnisms
Kvasir-SEG	10
ClinicDB	
BKAI	
CVC-300	
CVC-ColonDB	
ETIS	
ISIC	
DFU	
CAMUS	8
BUSI	7
CheXlocalize	
<b>Total</b>	<b>25</b>

In the experimental context, we utilized eleven datasets to address various segmentation tasks with 25 prompting mechanisms, as given in Table 6. The prompts remain essentially the same for the non-radiology images with slight variations, explained in Appendix B.2.1. Consequently, we had 102 zero-shot segmentation tasks for each model (CRIS [46] and CLIPSeg [27]), as shown in Appendix D.1. We used a pretrained version of CRIS for all zero-shot segmentation tasks and an initial checkpoint for fine-tuning. There has not been an official release of pretrained CRIS till the point of writing this document, so we used an unofficial checkpoint of the model shared in the issue in CRIS’ GitHub <sup>4</sup>. We employed four models for decoder training and fine-tuning: CRIS, CLIPSeg, BiomedCLIPSeg-D, and BiomedCLIPSeg. Each model had 82 training tasks because three datasets (CVC-300, CVC-ColonDB, and ETIS ) were excluded due to insufficient training data, as depicted in Appendix D.2.

Due to their differing decoder architectures, we selected CLIPSeg and CRIS for further pooled training, fine-tuning, and cross-endoscopy validation experiments. To assess the performance of the fine-tuned polyp segmentation model, we conducted evaluations by training it on one distribution and testing it on another as indicated in Appendix D.3. For pooled training, we explored selected prompting

<sup>4</sup><https://github.com/DerrickWang005/CRIS.pytorch/issues/3>



mechanisms from a mixed pool dataset dedicated to polyp segmentation as shown in Appendix D.4.1. Additionally, we conducted fine-tuning using a pooled dataset containing a combination of all 11 radiology and non-radiology images and evaluated them on individual datasets as presented in Appendix D.4.2. In this case, we randomly select a prompt for each image.

Lastly, we analyze if the models are over- or under-segmenting the prediction of the segmentation masks by comparing the corresponding models with a naive classifier that predicts every pixel as a foreground in Appendix E.

## D Results

### D.1 Zero-Shot Segmentation

For zero-shot segmentation tasks, we evaluated all 11 datasets considering their prompting mechanisms with two models of CRIS and CLIPSeg as shown in Tables 7 and 8 respectively.

Table 7: Zero-shot segmentation dice score of pre-trained CRIS on different datasets on different sets of prompts.

Prompt → Dataset ↓	P0	P1	P2	P3	P4	P5	P6	P7	P8	P9
Kvasir-SEG	36.1 $\pm$ 25.45	31.12 $\pm$ 19.78	42.48 $\pm$ 31.83	40.95 $\pm$ 33.73	49.94 $\pm$ 32.08	<b>51.04</b> $\pm$ 34.42	45.3 $\pm$ 35.82	23.31 $\pm$ 33.24	38.56 $\pm$ 37.61	38.56 $\pm$ 37.61
ClinicDB	23.98 $\pm$ 19.83	21.89 $\pm$ 15.71	32.09 $\pm$ 32.5	32.15 $\pm$ 29.19	40.3 $\pm$ 34.11	<b>40.88</b> $\pm$ 33.74	36.67 $\pm$ 37.69	15.21 $\pm$ 30.29	27.89 $\pm$ 37.37	27.9 $\pm$ 37.37
BKAI	14.43 $\pm$ 16.13	11.03 $\pm$ 9.79	13.64 $\pm$ 18.97	20.19 $\pm$ 24.87	31.98 $\pm$ 34.16	35.24 $\pm$ 35.5	<b>35.9</b> $\pm$ 37.91	14.93 $\pm$ 30.6	33.74 $\pm$ 38.32	33.75 $\pm$ 38.31
CVC-300	7.86 $\pm$ 5.84	7.87 $\pm$ 5.68	11.69 $\pm$ 12.78	14.28 $\pm$ 15.5	29.83 $\pm$ 32.16	28.93 $\pm$ 31.69	<b>38.9</b> $\pm$ 36.95	27.07 $\pm$ 36.43	33.64 $\pm$ 38.63	33.64 $\pm$ 38.63
CVC-Colondb	15.86 $\pm$ 17.7	16.46 $\pm$ 18.85	18.31 $\pm$ 22.38	18.94 $\pm$ 23.37	30.34 $\pm$ 31.48	30.8 $\pm$ 32.28	<b>34.73</b> $\pm$ 36.48	19.57 $\pm$ 30.83	29.2 $\pm$ 36.48	29.2 $\pm$ 36.48
ETIS	10.72 $\pm$ 14.58	9.61 $\pm$ 12.6	13.38 $\pm$ 23.26	16.9 $\pm$ 24.85	23.05 $\pm$ 30.02	23.42 $\pm$ 30.56	<b>24.88</b> $\pm$ 33.15	5.76 $\pm$ 17.62	22.11 $\pm$ 32.81	22.11 $\pm$ 32.81
ISIC	56.95 $\pm$ 31.55	63.8 $\pm$ 30.7	57.59 $\pm$ 33.61	60.66 $\pm$ 34.25	<b>66.07</b> $\pm$ 30.9	62.92 $\pm$ 32.22	61.79 $\pm$ 31.13	60.12 $\pm$ 33.06	61.93 $\pm$ 32.05	57.37 $\pm$ 32.18
DFU	9.67 $\pm$ 12.56	7.84 $\pm$ 17.09	8.24 $\pm$ 16.74	12.79 $\pm$ 20.26	11.5 $\pm$ 19.1	14.34 $\pm$ 20.85	12.81 $\pm$ 21.95	<b>18.49</b> $\pm$ 25.2	18.28 $\pm$ 25.4	18.28 $\pm$ 25.4
CAMUS	<b>23.53</b> $\pm$ 11.99	9.04 $\pm$ 13.87	8.36 $\pm$ 13.2	8.24 $\pm$ 13.2	8.24 $\pm$ 13.2	8.24 $\pm$ 13.2	8.24 $\pm$ 13.2	5.45 $\pm$ 10.41	N/A	N/A
BUSI	41.57 $\pm$ 35.71	45.41 $\pm$ 37.24	34.27 $\pm$ 36.78	46.12 $\pm$ 37.32	47.23 $\pm$ 35.44	<b>50.04</b> $\pm$ 35.19	48.74 $\pm$ 35.19	N/A	N/A	N/A
CheXlocalize	15.01 $\pm$ 13.48	17.10 $\pm$ 14.76	<b>18.08</b> $\pm$ 15.91	17.37 $\pm$ 17.29	15.73 $\pm$ 16.13	15.73 $\pm$ 16.13	15.75 $\pm$ 15.34	N/A	N/A	N/A

**Endoscopic Dataset** Table 7 shows that adding attributes in promoting up to **p6** has improved segmentation performance for endoscopic datasets. Addition of information about numbers (**p5**) and location (**p6**) seems to have helped CRIS the most with these datasets. In contrast, the general description of the class (**p7**) has degraded the performance in these. This could mean that the choice of descriptions we made for endoscopic datasets did not help the model look for appropriate areas in the image and probably confused it even more. Likewise, Table 8 shows that the addition of information about the shape (**p2**) of the target has helped the model the most in non-radiology images.

**Skin Dataset** For the ISIC [10] dataset, adding information about size (**p4**) has helped the model the most. And the dataset, in general, seems to appear with a more discriminative region to segment than others, resulting in reasonably good performance across every prompt.

**Foot Ulcer Dataset** For the DFU-2022 dataset [20], the general description (**p7**, **p8**, and **p9**) seems to have helped somewhat. This could be because there is a lot of reference to “foot” and “skin” in these descriptions. There is a high chance that the model might have been familiar with these in natural images compared to internal anatomical descriptions in endoscopy images.

**CAMUS Dataset** Both models performed poorly for the CAMUS dataset. CRIS’ performance is reduced by adding extra information to the prompt even if the dataset has multiple classes (a single image can have three plausible segmentation masks depending on what is being segmented). This clearly shows the over-segmenting tendency of **P0** and the under-segmenting tendency of other prompts. This can also be inferred from Figure 6. Similarly, CLIPSeg has an under-segmenting tendency for all the prompts (virtually all zeros), making the dice for each prompt near zero.

### D.2 Fine-tuned Segmentation

We have discarded CVC-300 [44], CVC-ColonDB [42], and ETIS [40] datasets for fine-tuning tasks because they have insufficient training data. The four models considered for fine-tuning are CRIS, CLIPSeg, BiomedCLIPSeg-D, and BiomedCLIPSeg, with their results shown in the Tables 9 to 12, respectively.

Table 8: Zero-shot segmentation dice score of pre-trained CLIPSeg on different datasets on different sets of prompts. The best combination of attributes for a prompt seems to depend on the dataset and the model for a zero-shot setting.

Prompt → Dataset ↓	P0	P1	P2	P3	P4	P5	P6	P7	P8	P9
Kvasir-SEG	8.23 $\pm$ 19.87	54.05 $\pm$ 30.47	<b>56.08</b> $\pm$ 31.29	40.02 $\pm$ 34.53	30.22 $\pm$ 33.64	32.01 $\pm$ 34.01	35.12 $\pm$ 35.41	55.8 $\pm$ 32.04	38.44 $\pm$ 35.89	36.55 $\pm$ 35.73
ClinicDB	18.68 $\pm$ 26.18	36.92 $\pm$ 30.78	<b>38.89</b> $\pm$ 34.35	31.12 $\pm$ 34.67	29.72 $\pm$ 35.34	33.17 $\pm$ 35.85	30.6 $\pm$ 34.25	39.3 $\pm$ 34.75	31.68 $\pm$ 35.07	28.6 $\pm$ 32.91
BKAI	2.73 $\pm$ 12.6	30.13 $\pm$ 34.01	<b>32.93</b> $\pm$ 37.07	24.97 $\pm$ 34.61	25.12 $\pm$ 35.42	24.93 $\pm$ 35.72	24.27 $\pm$ 35.31	28.47 $\pm$ 36.47	26.3 $\pm$ 36.62	24.32 $\pm$ 35.06
CVC-300	3.94 $\pm$ 14.59	15.06 $\pm$ 21.39	<b>33.68</b> $\pm$ 35.39	29.31 $\pm$ 35.43	23.69 $\pm$ 34.99	20.1 $\pm$ 32.98	28.66 $\pm$ 38.62	1.53 $\pm$ 6.59	33.2 $\pm$ 37.45	30.03 $\pm$ 38.32
CVC-ColonDB	6.15 $\pm$ 17.85	20.61 $\pm$ 27.37	<b>25.88</b> $\pm$ 30.22	22.06 $\pm$ 30.42	19.92 $\pm$ 31.25	19.18 $\pm$ 30.61	18.51 $\pm$ 30.62	12.32 $\pm$ 24.94	21.8 $\pm$ 32.16	18.72 $\pm$ 30.83
ETIS	3.57 $\pm$ 13.28	20.00 $\pm$ 31.59	20.26 $\pm$ 32.59	16.01 $\pm$ 27.7	12.92 $\pm$ 27.38	13.23 $\pm$ 27.56	13.51 $\pm$ 27.77	<b>20.87</b> $\pm$ 32.28	14.46 $\pm$ 28.25	15.15 $\pm$ 28.93
ISIC	16.29 $\pm$ 27.85	22.52 $\pm$ 34.12	64.11 $\pm$ 33.73	65.67 $\pm$ 32.47	64.06 $\pm$ 33.1	61.83 $\pm$ 35.07	64.26 $\pm$ 31.97	38.10 $\pm$ 37.05	59.88 $\pm$ 35.48	<b>67.98</b> $\pm$ 31.09
DFU	3.09 $\pm$ 12.57	0.57 $\pm$ 1.95	0.56 $\pm$ 3.62	0.43 $\pm$ 3.05	0.38 $\pm$ 2.89	0.33 $\pm$ 2.55	<b>3.41</b> $\pm$ 11.04	0.19 $\pm$ 0.99	0.05 $\pm$ 0.61	0.47 $\pm$ 2.84
CAMUS	0.00 $\pm$ 0.00	0.00 $\pm$ 0.00	0.21 $\pm$ 1.79	0.16 $\pm$ 1.85	0.19 $\pm$ 2.11	<b>0.51</b> $\pm$ 3.67	0.46 $\pm$ 3.13	1.81 $\pm$ 6.58	N/A	N/A
BUSI	<b>27.97</b> $\pm$ 38.6	22.59 $\pm$ 36.44	24.18 $\pm$ 37.01	20.61 $\pm$ 36.77	19.41 $\pm$ 37.16	18.95 $\pm$ 37.16	27.95 $\pm$ 37.43	N/A	N/A	N/A
CheXlocalize	<b>0.52</b> $\pm$ 3.959	0.00 $\pm$ 0.00	0.00 $\pm$ 0.00	0.00 $\pm$ 0.00	0.00 $\pm$ 0.00	0.00 $\pm$ 0.00	0.00 $\pm$ 0.00	N/A	N/A	N/A

Table 9: Fine-tuned segmentation dice score of CRIS on different datasets on different sets of prompts.

Prompt → Dataset ↓	P0	P1	P2	P3	P4	P5	P6	P7	P8	P9
Kvasir-SEG	0.0 $\pm$ 0	0.07 $\pm$ 0.67	83.61 $\pm$ 20.18	83.49 $\pm$ 23.09	85.73 $\pm$ 18.93	86.14 $\pm$ 18.42	<b>86.52</b> $\pm$ 16.67	84.64 $\pm$ 21.76	86.08 $\pm$ 16.84	82.29 $\pm$ 23.03
ClinicDB	0.0 $\pm$ 0	22.72 $\pm$ 22.41	81.18 $\pm$ 24.11	80.82 $\pm$ 23.92	83.08 $\pm$ 24.86	<b>84.62</b> $\pm$ 20.0	79.55 $\pm$ 27.97	83.4 $\pm$ 22.88	82.67 $\pm$ 22.32	83.27 $\pm$ 22.5
BKAI	0.0 $\pm$ 0	73.18 $\pm$ 28.28	82.66 $\pm$ 23.41	83.5 $\pm$ 23.48	83.24 $\pm$ 24.83	83.03 $\pm$ 24.63	<b>84.06</b> $\pm$ 22.66	83.17 $\pm$ 23.89	83.15 $\pm$ 24.61	83.88 $\pm$ 24.04
ISIC	2.46 $\pm$ 6.55	88.46 $\pm$ 13.73	89.04 $\pm$ 12.78	89.23 $\pm$ 11.88	88.54 $\pm$ 12.84	89.14 $\pm$ 11.96	88.41 $\pm$ 13.45	89.05 $\pm$ 11.66	<b>89.38</b> $\pm$ 11.59	
DFU	0.58 $\pm$ 3.09	14.75 $\pm$ 19.58	69.62 $\pm$ 26.76	68.32 $\pm$ 28.23	68.22 $\pm$ 27.57	68.13 $\pm$ 28.21	<b>71.01</b> $\pm$ 26.68	70.35 $\pm$ 27.31	68.97 $\pm$ 27.83	69.85 $\pm$ 26.86
CAMUS	2.94 $\pm$ 8.12	<b>94.04</b> $\pm$ 6.25	93.38 $\pm$ 6.09	91.68 $\pm$ 6.98	86.15 $\pm$ 12.58	87.75 $\pm$ 9.82	87.62 $\pm$ 10.03	87.48 $\pm$ 10.01	N/A	N/A
BUSI	31.15 $\pm$ 23.67	76.89 $\pm$ 25.76	77.58 $\pm$ 24.69	74.27 $\pm$ 28.67	78.82 $\pm$ 25.27	79.89 $\pm$ 22.09	<b>80.64</b> $\pm$ 21.55	N/A	N/A	N/A
CheXlocalize	0.02 $\pm$ 0.23	55.87 $\pm$ 26.6	56.36 $\pm$ 26.24	56.17 $\pm$ 26.93	58.17 $\pm$ 25.64	<b>59.21</b> $\pm$ 24.79	56.18 $\pm$ 26.02	N/A	N/A	N/A

Table 10: Fine-tuned segmentation dice score of CLIPSeg on different datasets on different sets of prompts.

Prompt → Dataset ↓	P0	P1	P2	P3	P4	P5	P6	P7	P8	P9
Kvasir-SEG	86.9 $\pm$ 16.54	86.2 $\pm$ 16.24	86.69 $\pm$ 16.23	87.39 $\pm$ 15.3	88.66 $\pm$ 11.35	88.2 $\pm$ 13.94	<b>89.1</b> $\pm$ 11.74	87.74 $\pm$ 14.39	89.0 $\pm$ 11.97	88.08 $\pm$ 13.34
ClinicDB	88.22 $\pm$ 15.56	88.38 $\pm$ 14.06	88.5 $\pm$ 13.86	88.84 $\pm$ 12.0	89.58 $\pm$ 10.23	89.98 $\pm$ 10.48	<b>90.28</b> $\pm$ 9.21	88.91 $\pm$ 11.47	89.04 $\pm$ 11.35	88.24 $\pm$ 13.16
BKAI	83.56 $\pm$ 19.68	84.63 $\pm$ 16.45	83.97 $\pm$ 17.73	<b>85.22</b> $\pm$ 16.02	83.97 $\pm$ 18.42	84.83 $\pm$ 16.06	84.91 $\pm$ 16.91	84.05 $\pm$ 18.32	84.46 $\pm$ 16.74	84.07 $\pm$ 18.46
ISIC	91.66 $\pm$ 9.47	92.05 $\pm$ 7.52	91.7 $\pm$ 9.12	91.45 $\pm$ 9.07	92.19 $\pm$ 6.96	91.88 $\pm$ 7.95	91.91 $\pm$ 7.71	91.96 $\pm$ 7.69	92.03 $\pm$ 7.34	<b>92.23</b> $\pm$ 7.53
DFU	71.43 $\pm$ 24.35	72.22 $\pm$ 25.52	72.16 $\pm$ 25.29	72.32 $\pm$ 24.57	72.25 $\pm$ 24.75	72.58 $\pm$ 25.02	73.56 $\pm$ 24.23	72.3 $\pm$ 24.74	73.24 $\pm$ 24.53	<b>73.58</b> $\pm$ 24.04
CAMUS	46.34 $\pm$ 13.93	88.29 $\pm$ 8.02	88.37 $\pm$ 8.04	88.41 $\pm$ 7.62	88.48 $\pm$ 7.76	88.25 $\pm$ 7.9	<b>88.51</b> $\pm$ 7.41	87.82 $\pm$ 9.02	N/A	N/A
BUSI	63.39 $\pm$ 38.44	64.33 $\pm$ 38.8	63.62 $\pm$ 38.13	62.79 $\pm$ 38.97	62.49 $\pm$ 38.54	<b>65.02</b> $\pm$ 37.43	64.86 $\pm$ 37.73	N/A	N/A	N/A
CheXlocalize	45.66 $\pm$ 25.45	58.31 $\pm$ 24.41	<b>59.30</b> $\pm$ 24.27	57.98 $\pm$ 24.50	57.76 $\pm$ 25.99	58.84 $\pm$ 24.78	58.54 $\pm$ 24.78	N/A	N/A	N/A

Table 11: Fine-tuned segmentation dice score of BiomedCLIPSeg-D on different datasets on different sets of prompts.

Prompt → Dataset ↓	P0	P1	P2	P3	P4	P5	P6	P7	P8	P9
Kvasir-SEG	71.71 $\pm$ 22.82	73.97 $\pm$ 22.0	70.83 $\pm$ 25.36	72.37 $\pm$ 23.11	74.23 $\pm$ 24.53	<b>74.66</b> $\pm$ 21.36	74.59 $\pm$ 23.31	72.23 $\pm$ 23.99	74.47 $\pm$ 22.93	73.63 $\pm$ 22.71
ClinicDB	71.16 $\pm$ 24.32	70.99 $\pm$ 24.69	72.55 $\pm$ 25.18	71.81 $\pm$ 23.12	72.31 $\pm$ 24.22	71.04 $\pm$ 25.75	73.09 $\pm$ 23.86	<b>73.76</b> $\pm$ 21.78	71.67 $\pm$ 24.58	72.91 $\pm$ 24.03
BKAI	64.81 $\pm$ 29.05	62.86 $\pm$ 28.95	<b>65.54</b> $\pm$ 28.27	62.52 $\pm$ 28.99	63.97 $\pm$ 31.5	64.87 $\pm$ 28.84	63.26 $\pm$ 30.57	64.99 $\pm$ 29.11	64.94 $\pm$ 28.31	64.92 $\pm$ 28.71
ISIC	89.3 $\pm$ 10.04	89.19 $\pm$ 10.64	89.37 $\pm$ 10.21	89.44 $\pm$ 10.21	<b>89.98</b> $\pm$ 8.95	89.78 $\pm$ 9.65	89.81 $\pm$ 9.51	89.27 $\pm$ 10.1	89.67 $\pm$ 9.64	89.53 $\pm$ 9.51
DFU	59.01 $\pm$ 28.57	58.4 $\pm$ 30.12	57.96 $\pm$ 29.32	59.12 $\pm$ 28.4	58.32 $\pm$ 29.26	59.13 $\pm$ 28.73	58.8 $\pm$ 30.26	<b>59.26</b> $\pm$ 29.68	59.03 $\pm$ 29.37	57.7 $\pm$ 29.1
CAMUS	45.82 $\pm$ 14.21	85.09 $\pm$ 9.99	85.29 $\pm$ 9.33	85.63 $\pm$ 9.41	85.26 $\pm$ 9.66	85.51 $\pm$ 9.26	85.46 $\pm$ 9.97	<b>85.69</b> $\pm$ 10.7	N/A	N/A
BUSI	60.59 $\pm$ 33.98	60.4 $\pm$ 34.2	61.63 $\pm$ 35.3	<b>63.17</b> $\pm$ 34.83	57.27 $\pm$ 34.08	61.73 $\pm$ 34.94	53.71 $\pm$ 33.63	N/A	N/A	N/A
CheXlocalize	42.03 $\pm$ 25.01	47.76 $\pm$ 26.04	<b>48.82</b> $\pm$ 26.26	48.76 $\pm$ 26.56	48.41 $\pm$ 26.68	48.08 $\pm$ 26.84	46.69 $\pm$ 26.72	N/A	N/A	N/A

Table 12: Fine-tuned segmentation dice score of BiomedCLIPSeg on different datasets on different sets of prompts.

Prompt → Dataset ↓	P0	P1	P2	P3	P4	P5	P6	P7	P8	P9
Kvasir-SEG	79.43 $\pm$ 19.73	80.83 $\pm$ 19.46	79.77 $\pm$ 20.22	80.32 $\pm$ 18.18	82.7 $\pm$ 18.34	82.11 $\pm$ 17.25	81.79 $\pm$ 19.29	78.84 $\pm$ 22.08	80.86 $\pm$ 17.85	<b>82.05</b> $\pm$ 17.99
ClinicDB	84.1 $\pm$ 14.73	84.61 $\pm$ 16.56	84.32 $\pm$ 14.47	<b>85.38</b> $\pm$ 12.44	82.79 $\pm$ 15.61	83.1 $\pm$ 16.17	83.47 $\pm$ 16.93	83.21 $\pm$ 19.67	83.82 $\pm$ 14.33	84.52 $\pm$ 14.23
BKAI	75.67 $\pm$ 22.22	75.56 $\pm$ 21.16	75.46 $\pm$ 20.97	75.32 $\pm$ 20.36	76.8 $\pm$ 21.09	<b>77.7</b> $\pm$ 19.32	76.92 $\pm$ 20.72	76.6 $\pm$ 20.31	76.52 $\pm$ 19.8	76.01 $\pm$ 21.15
ISIC	90.89 $\pm$ 9.08	90.67 $\pm$ 9.01	90.95 $\pm$ 8.76	90.81 $\pm$ 9.28	91.23 $\pm$ 8.63	<b>91.65</b> $\pm$ 8.17	91.45 $\pm$ 8.82	90.77 $\pm$ 9.42	91.44 $\pm$ 7.96	91.31 $\pm$ 8.74
DFU	65.72 $\pm$ 25.74	65.02 $\pm$ 26.81	<b>66.24</b> $\pm$ 26.78	65.46 $\pm$ 27.2	66.17 $\pm$ 26.66	65.64 $\pm$ 27.13	65.0 $\pm$ 27.58	64.52 $\pm$ 27.53	65.75 $\pm$ 27.04	65.9 $\pm$ 26.53
CAMUS	45.84 $\pm$ 15.63	86.64 $\pm$ 10.1	86.56 $\pm$ 9.67	87.06 $\pm$ 9.08	86.9 $\pm$ 9.33	87.03 $\pm$ 9.16	87.05 $\pm$ 9.16	<b>87.24</b> $\pm$ 8.42	N/A	N/A
BUSI	62.19 $\pm$ 35.59	64.25 $\pm$ 35.82	62.31 $\pm$ 35.12	63.23 $\pm$ 35.83	65.20 $\pm$ 35.35	<b>64.71</b> $\pm$ 36.58	64.03 $\pm$ 36.65	N/A	N/A	N/A
CheXlocalize	44.81 $\pm$ 25.66	57.45 $\pm$ 25.51	57.84 $\pm$ 24.26	57.75 $\pm$ 24.68	<b>58.06</b> $\pm$ 25.01	57.68 $\pm$ 25.01	58.01 $\pm$ 24.97	N/A	N/A	N/A

### D.3 Cross-Endoscopy Validation

There are a total of six endoscopy datasets with polyp segmentation masks. For cross-endoscopy validation, we have considered the models fine-tuned on one of the endoscopy datasets (Kvasir-SEG, ClinicDB, and BKAI) in Appendix D.2 and evaluated them on other five endoscopy datasets. The

models considered for these evaluation tasks are CRIS and CLIPSeg, with their results presented in Tables 13 to 18.

Table 13: Dice score of CRIS model fine-tuned on Kvasir-SEG and tested on other endoscopy datasets.

Prompt → Dataset ↓	P0	P1	P2	P3	P4	P5	P6	P7	P8	P9
ClinicDB	0.0±0	0.0±0.0	70.94±28.86	71.23±31.43	72.35±27.11	<b>74.21</b> ±27.63	73.82±27.88	70.39±30.86	72.91±28.91	69.78±31.14
BKAI	0.0±0	0.04±0.39	63.26±38.4	64.3±37.93	67.34±37.99	66.57±38.63	<b>69.32</b> ±36.91	66.05±38.83	68.01±38.22	59.38±41.1
CVC-300	0.0±0.0	0.0±0.0	71.32±25.45	74.75±25.48	77.49±21.71	80.27±20.89	<b>81.61</b> ±18.19	75.86±25.72	80.27±23.97	74.32±25.44
CVC-Colondb	0.0±0.0	0.0±0.01	56.51±36.21	57.18±36.91	64.24±34.45	64.4±35.77	<b>67.51</b> ±32.52	57.78±37.57	64.02±36.44	59.03±36.96
ETIS	0.0±0.0	0.0±0.0	37.43±39.49	42.44±39.06	<b>47.84</b> ±39.73	47.78±40.11	46.74±38.94	40.31±41.39	43.04±41.73	37.37±40.55

Table 14: Dice score of CRIS model fine-tuned on ClinicDB and tested on other endoscopy datasets.

Prompt → Dataset ↓	P0	P1	P2	P3	P4	P5	P6	P7	P8	P9
Kvasir-SEG	36.21±25.61	9.33±16.24	75.12±26.83	75.07±26.46	78.77±23.97	79.56±20.51	78.76±22.48	78.11±23.75	77.58±23.17	<b>79.74</b> ±22.49
BKAI	23.55±26.08	8.26±14.11	63.84±35.98	63.05±36.03	<b>69.69</b> ±33.63	69.22±33.72	64.98±34.42	64.14±35.77	68.15±35.09	67.04±35.62
CVC 300	15.52±21.42	17.48±19.72	79.53±22.06	79.2±20.79	80.53±23.45	80.06±24.29	<b>84.04</b> ±16.93	77.34±26.9	81.97±19.72	77.33±28.79
CVC Colondb	20.38±23.39	9.58±15.52	61.03±37.52	60.66±36.28	64.85±34.59	66.17±34.68	<b>67.78</b> ±33.21	59.8±37.3	66.85±33.75	66.37±34.81
ETIS	13.59±21.08	8.03±15.2	41.38±39.05	43.06±37.85	50.14±38.27	51.52±36.86	52.32±35.65	44.79±38.67	51.95±36.89	<b>53.36</b> ±37.39

Table 15: Dice score of CRIS model fine-tuned on BKAI and tested on other endoscopy datasets.

Prompt → Dataset ↓	P0	P1	P2	P3	P4	P5	P6	P7	P8	P9
Kvasir-SEG	39.85±20.55	52.81±31.35	76.8±26.98	73.9±28.29	77.01±26.21	77.59±27.64	74.91±28.45	76.12±27.66	79.38±25.5	<b>79.61</b> ±25.28
Clinicdb	26.67±17.89	64.64±33.89	68.81±32.43	68.2±34.67	71.43±32.35	70.56±32.71	68.13±33.89	67.68±34.54	<b>71.43</b> ±32.05	70.34±32.41
CVC 300	24.00±21.86	75.79±28.21	81.21±22.04	80.33±23.26	78.57±25.96	79.29±25.41	<b>83.55</b> ±16.83	80.21±25.92	82.25±22.23	82.11±20.96
CVC Colondb	23.28±21.37	44.9±37.37	56.6±38.4	55.44±38.99	58.01±37.83	58.92±37.75	<b>64.58</b> ±34.55	56.83±39.43	58.49±37.65	57.1±38.31
ETIS	39.21±35.8	39.21±35.8	47.74±38.92	51.93±37.18	55.85±36.79	56.57±37.23	<b>59.82</b> ±34.37	52.65±37.68	56.86±37.59	54.77±37.97

Table 16: Dice score of CLIPSeg model fine-tuned on Kvasir-SEG and tested on other endoscopy datasets.

Prompt → Dataset ↓	P0	P1	P2	P3	P4	P5	P6	P7	P8	P9
ClinicDB	79.26±25.26	80.02±22.84	78.56±25.31	78.28±25.97	<b>80.52</b> ±22.56	80.26±23.24	78.42±25.65	79.02±25.07	79.64±22.73	79.85±23.44
BKAI	75.17±26.86	75.09±27.29	76.34±25.62	76.04±27.13	77.01±27.59	77.25±27.11	74.17±31.55	76.84±26.12	<b>78.0</b> ±23.43	77.76±24.04
CVC-300	85.97±13.9	85.57±14.28	83.35±17.08	81.43±24.46	83.21±17.9	<b>86.37</b> ±12.71	84.34±17.55	84.76±14.58	83.95±17.46	86.0±13.0
CVC-ColonDB	67.74±31.41	68.82±30.12	69.03±29.44	68.24±30.98	<b>71.55</b> ±27.46	71.24±29.04	68.35±31.36	70.09±29.59	70.19±28.3	70.39±29.77
ETIS	59.3±34.67	60.41±33.13	60.78±33.1	59.08±34.79	61.6±32.67	61.94±34.11	57.42±36.2	60.93±32.95	59.95±32.7	<b>61.79</b> ±34.02

Table 17: Dice score of CLIPSeg model fine-tuned on ClinicDB and tested on other endoscopy datasets.

Prompt → Dataset ↓	P0	P1	P2	P3	P4	P5	P6	P7	P8	P9
Kvasir-SEG	81.25±19.86	81.87±19.19	81.25±19.89	83.13±17.0	83.92±15.51	82.87±18.11	<b>84.15</b> ±16.07	81.88±19.26	83.65±18.06	83.49±16.87
BKAI	68.59±32.18	70.71±29.56	71.62±29.36	<b>73.55</b> ±27.58	73.28±27.81	72.68±28.96	70.24±30.39	70.96±30.48	73.46±27.71	72.71±28.6
CVC-300	85.22±15.9	86.95±13.03	85.27±15.04	87.64±12.94	<b>87.91</b> ±12.49	87.31±13.85	87.49±13.6	86.43±14.15	87.39±13.98	87.26±13.67
CVC-ColonDB	66.31±31.07	67.32±30.69	67.2±30.89	68.65±29.95	<b>70.29</b> ±29.07	67.96±30.44	69.81±29.68	67.27±30.39	69.47±28.71	69.29±29.09
ETIS	57.48±35.47	58.26±34.09	59.67±34.27	<b>61.23</b> ±32.11	59.66±33.49	60.09±34.01	60.34±33.7	59.33±34.64	60.92±33.38	60.04±32.99

Table 18: Dice score of CLIPSeg model fine-tuned on BKAI and tested on other endoscopy datasets.

Prompt → Dataset ↓	P0	P1	P2	P3	P4	P5	P6	P7	P8	P9
Kvasir-SEG	82.32±18.74	81.78±18.5	81.97±17.73	81.28±18.93	<b>84.62</b> ±17.46	81.91±17.81	82.42±19.16	79.2±20.31	83.64±18.99	82.43±19.67
ClinicDB	75.37±26.95	73.69±28.53	75.27±25.0	73.31±28.4	<b>76.37</b> ±26.13	73.42±27.23	76.17±25.5	73.45±28.31	76.28±25.77	71.11±30.13
CVC-300	82.69±19.43	80.88±23.81	81.25±18.9	82.52±16.61	<b>83.26</b> ±19.37	82.04±21.24	83.26±21.89	81.49±22.47	81.6±21.63	80.89±22.99
CVC-ColonDB	63.19±34.32	60.24±34.49	60.73±32.99	60.76±33.98	62.5±34.34	60.41±33.87	<b>63.66</b> ±33.78	60.26±34.15	63.23±33.25	57.3±35.23
ETIS	62.6±33.52	62.03±32.08	64.06±29.5	59.72±33.74	62.26±32.78	59.07±34.52	63.02±31.8	58.14±34.96	<b>64.09</b> ±31.61	58.1±34.35

We conducted these cross-dataset tests to observe how well prompting helps a model to generalize to datasets with different distributions. But we observe the performances in cross-dataset training and test to be poorer than within-dataset training and test. Another critical observation is whether models leverage adding attributes to prompts for adjusting across datasets of different distributions. The higher relative gain in performance compared to within-dataset tests on adding attributes to prompts in CRIS might indicate that CRIS has tried to leverage adding attributes to prompts to help in cross-dataset generalization. But in CLIPSeg, the effect does not seem to be as significant.

## D.4 Pooled Datasets Training

### D.4.1 Polyp-mixed

It is generally observed that models find it difficult to learn combinedly from datasets with different distributions. We conducted training by pooling different endoscopy datasets to observe whether leveraging textual information and visual help models learn from various datasets together.

For polyp-mixed validation, we have considered the models fine-tuned on the pool of three endoscopy datasets (Kvasir-SEG, ClinicDB, and BKAI) and evaluated them on the other five endoscopy datasets. The models considered for these evaluation tasks are CRIS and CLIPSeg, with their results presented in Tables 19 and 20.

Table 19: Dice score of CRIS model fine-tuned on the pool of three endoscopy datasets (Kvasir-SEG, ClinicDB, and BKAI) conducted considering only three main prompting mechanisms and one by selecting prompts randomly from every kind.

Prompt → Dataset ↓	P0	P6	P9	Random
Kvasir-SEG	14.61 $\pm$ 19.43	<b>89.41</b> $\pm$ 14.14	88.95 $\pm$ 14.91	87.73 $\pm$ 16.75
ClinicDB	18.43 $\pm$ 23.27	<b>85.99</b> $\pm$ 19.51	83.19 $\pm$ 24.16	83.90 $\pm$ 24.56
BKAI	13.67 $\pm$ 20.25	<b>85.29</b> $\pm$ 21.83	83.07 $\pm$ 25.21	83.84 $\pm$ 24.05
CVC-300	11.27 $\pm$ 19.73	85.39 $\pm$ 19.26	<b>86.03</b> $\pm$ 16.95	84.24 $\pm$ 18.83
CVC-ColonDB	6.81 $\pm$ 15.05	73.60 $\pm$ 30.55	<b>74.23</b> $\pm$ 29.98	68.53 $\pm$ 32.98
ETIS	3.67 $\pm$ 11.61	<b>71.73</b> $\pm$ 30.8	67.71 $\pm$ 32.84	65.41 $\pm$ 34.98

Table 20: Dice score of CLIPSeg model fine-tuned on the pool of three endoscopy datasets (Kvasir-SEG, ClinicDB, and BKAI) conducted considering only three main prompting mechanisms and one by selecting prompts randomly from every kind.

Prompt → Dataset ↓	P0	P6	P9	Random
Kvasir-SEG	87.11 $\pm$ 16.51	<b>89.01</b> $\pm$ 13.69	88.54 $\pm$ 14.62	88.03 $\pm$ 15.85
ClinicDB	<b>90.76</b> $\pm$ 7.77	90.23 $\pm$ 8.83	89.93 $\pm$ 11.69	86.95 $\pm$ 15.89
BKAI	<b>86.43</b> $\pm$ 13.79	84.78 $\pm$ 17.5	85.1 $\pm$ 17.3	84.38 $\pm$ 20.46
CVC-300	88.05 $\pm$ 12.6	88.2 $\pm$ 14.25	88.03 $\pm$ 12.87	<b>88.3</b> $\pm$ 9.61
CVC-ColonDB	72.43 $\pm$ 27.85	73.1 $\pm$ 28.19	<b>74.56</b> $\pm$ 27.15	69.81 $\pm$ 29.74
ETIS	66.44 $\pm$ 30.86	68.23 $\pm$ 31.29	<b>69.56</b> $\pm$ 29.95	67.65 $\pm$ 31.83

### D.4.2 All mixed

For all mixed validation, we considered the models fine-tuned on the pool of all datasets mentioned before and evaluated them on the test splits of their datasets. A single prompt used for an image has been sampled from the multiple prompts. The models considered for these evaluation tasks are CRIS and CLIPSeg, with their results presented in Table 21.

## D.5 Using radiology reports for lung segmentation

To examine the usage of using free-text radiology reports of chest x-ray for segmentation, we have utilized 1,141 frontal-view CXRs randomly selected from the MIMIC-CXR database [5, 18, 19]. This dataset contains the segmentation of lungs, which has been verified manually. We used the free-text radiology reports provided in the MIMIC-CXR Database [18] as the only prompt (P1).

Table 22 shows that in both CRIS and CLIPSeg models, adding reports as additional prompts negatively affects zero-shot segmentation. However, when fine-tuning, CRIS performs significantly better with reports than empty prompts. This indicates that adding only free-text radiology reports of the chest X-ray might benefit lung segmentation tasks.

Table 21: Dice score on different test splits of all datasets for the model fine-tuned on the pooled training set of all available datasets. CLIPSeg has a better performance than CRIS when they are trained on all the available datasets and evaluated on the test sets.

<b>Dataset</b> ↓ <b>Model</b> →	<b>CRIS</b>	<b>CLIPSeg</b>
<b>Kvasir-SEG</b>	<b>86.94</b> $\pm 16.58$	86.08 $\pm 16.96$
<b>ClinicDB</b>	84.49 $\pm 23.07$	<b>86.49</b> $\pm 15.7$
<b>BKAI</b>	82.8 $\pm 25.36$	<b>83.93</b> $\pm 18.36$
<b>CVC-300</b>	82.97 $\pm 19.3$	<b>91.47</b> $\pm 6.45$
<b>CVC-ColonDB</b>	68.17 $\pm 33.78$	<b>74.97</b> $\pm 27.67$
<b>ETIS</b>	60.95 $\pm 36.74$	<b>70.3</b> $\pm 31.04$
<b>ISIC</b>	91.11 $\pm 8.91$	<b>91.56</b> $\pm 8.93$
<b>DFU</b>	67.36 $\pm 29.28$	<b>71.43</b> $\pm 26.09$
<b>CAMUS</b>	81.26 $\pm 20.98$	<b>82.01</b> $\pm 17.67$
<b>BUSI</b>	<b>78.39</b> $\pm 29.4$	65.05 $\pm 37.1$
<b>CheXlocalize</b>	<b>56.19</b> $\pm 26.75$	54.64 $\pm 25.9$

Table 22: Zero-shot and fine-tuning dice scores of the CRIS and CLIPSeg Manually labeled Chest Xray Segmentation Dataset. We have used the actual radiology reports as **P1**. P0 indicates an empty prompt.

<b>Models</b>	<b>Experiment</b> ↓ <b>Prompt</b> →	<b>P0</b>	<b>P1</b>
<b>CRIS</b>	<b>Zero-shot</b>	<b>44.8</b> $\pm 18.97$	40.73 $\pm 18.95$
	<b>Fine-tuning</b>	81.66 $\pm 5.65$	<b>90.99</b> $\pm 1.41$
<b>CLIPSeg</b>	<b>Zero-shot</b>	<b>0.26</b> $\pm 2.35$	0.09 $\pm 0.88$
	<b>Fine-tuning</b>	<b>91.39</b> $\pm 1.09$	91.22 $\pm 1.26$

## E All Ones vs. Models' Predictions

### E.1 Zero-shot Setting

We found the models predicting the over-segmented masks in a zero-shot setting. So, we compared the performance of a model which predicts all the pixels as foreground with that of CRIS (Figure 6) and CLIPSeg (Figure 7).

### E.2 Finetuning

Figures 8 and 9 show the difference in dice for the predictions of the finetuned models and a naive model that predicts all the pixels as the foreground. As expected, the difference has increased than in the zero-shot setting, inferring the fine-tuned models have performed better than the naive model. Due to insufficient training data, we discarded CVC-300, CVC-ColonDB, and ETIS datasets for fine-tuning.

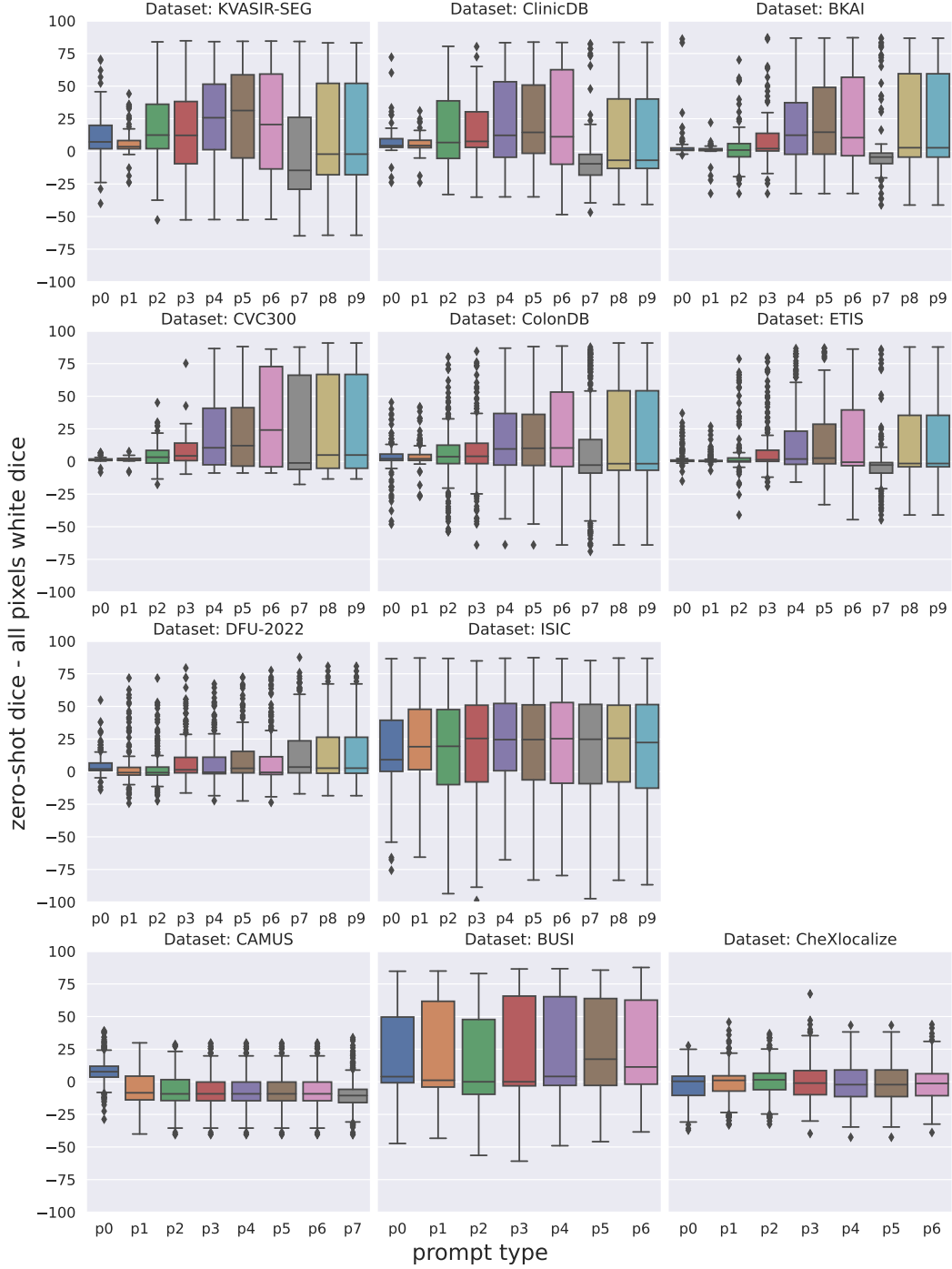


Figure 6: Zero-shot performance of CRIS across different datasets compared to a segmenter that segments every pixel as foreground. CRIS’ prediction for endoscopy datasets for some of the initial prompts seems to be the same as that of the all-one predictor. The naive predictor performed on par with CRIS for all the prompts for the DFU and CheXlocalize datasets. Also, CRIS performed poorer than the naive classifier for the CAMUS dataset, showing the tendency of CRIS to under-segment when the details in the prompt increase.

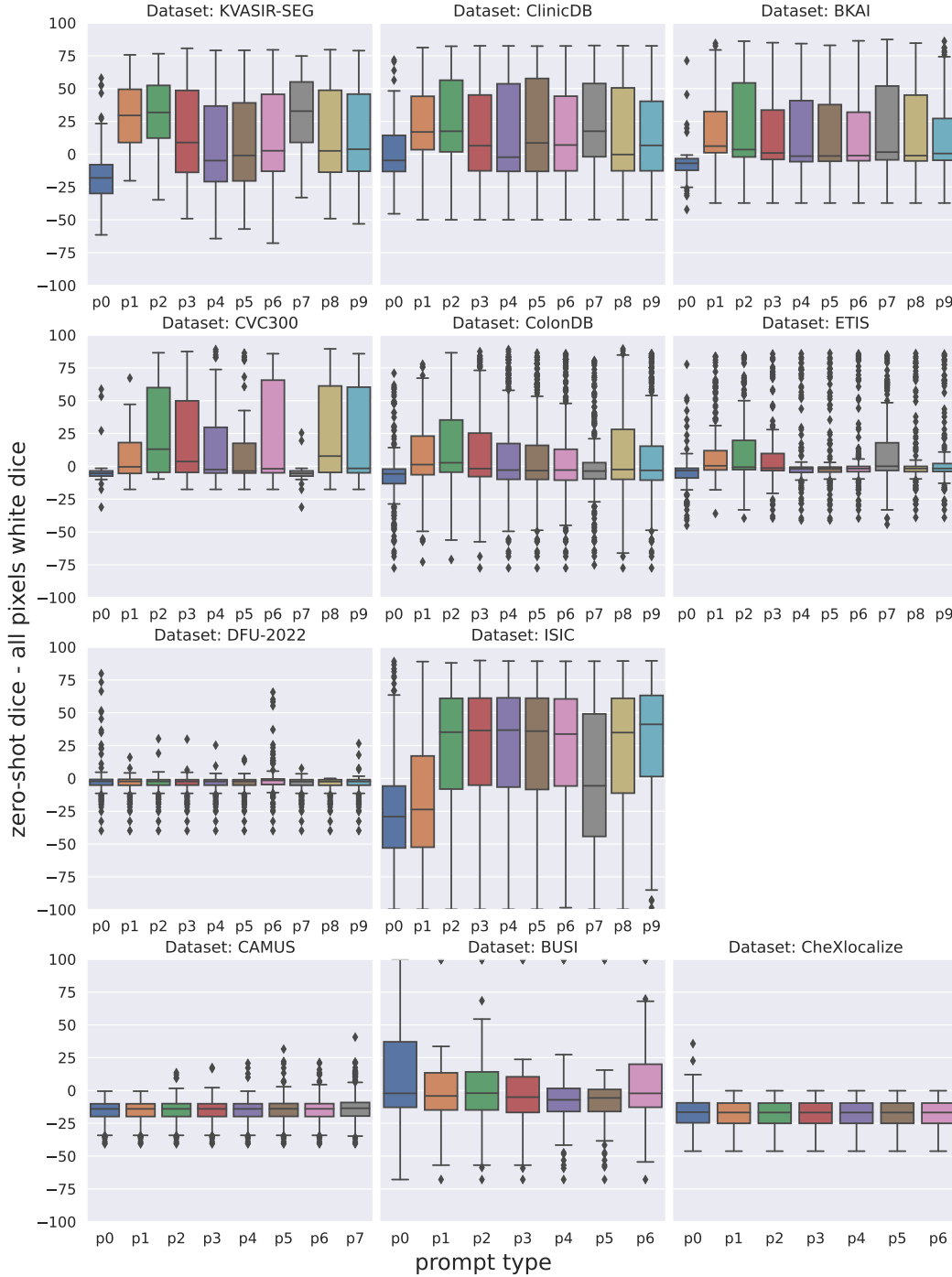


Figure 7: Zero-shot performance of CLIP-SEG across different datasets compared to a segmenter that segments every pixel as foreground. In the case of CLIPSeg, it performed on par with the all-one classifier for the ColonDB, ETIS, DFU, and BUSI. It performed poorer than the naive classifier for CAMUS, CheXlocalize, and the initial prompts of ISIC.

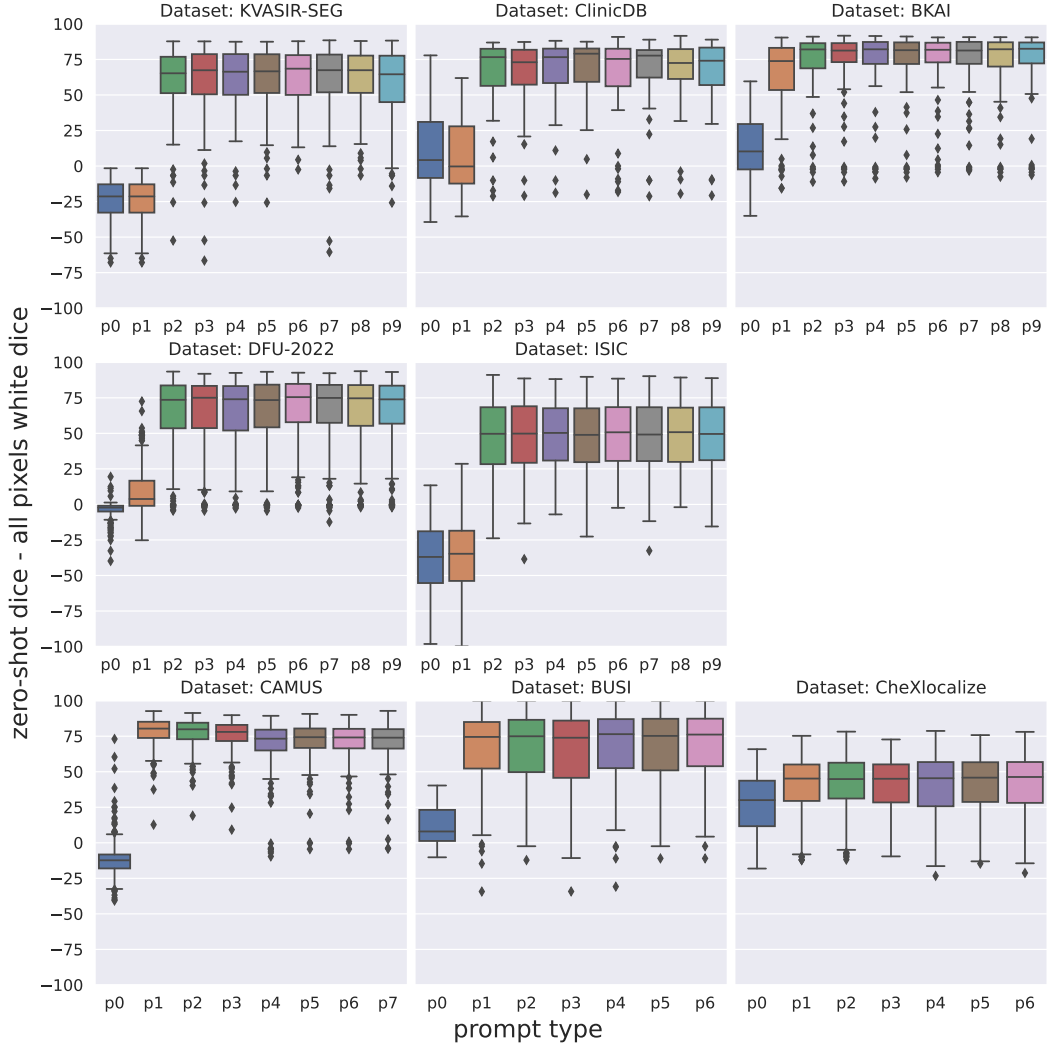


Figure 8: Fine-tuned performance of CRIS across different datasets compared to a model that segments every pixel as foreground. CRIS performs significantly better than the naive model, except for the empty prompt and the class keyword.



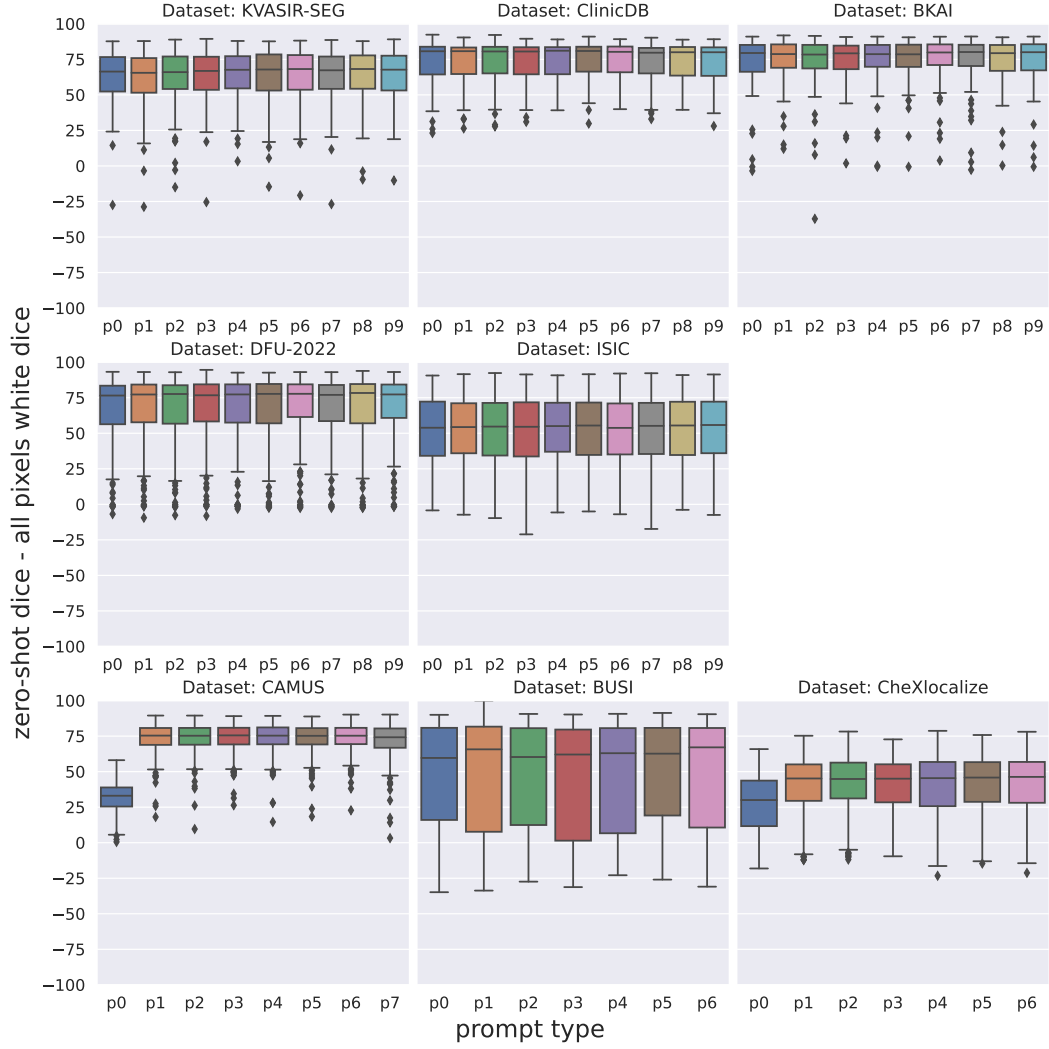


Figure 9: Fine-tuned performance of CLIPSeg across different datasets compared to a model that segments every pixel as foreground. CLIPSeg performs better than the naive model for all the datasets' prompts. The difference slightly decreases for CAMUS and CheXlocalize for the empty prompt. This may be because they are multi-class datasets, so the same image can have different segmentation masks depending on what is being segmented.